The Astrophysical Journal, 611:476–493, 2004 August 10

IS HE 0107−5240 A PRIMORDIAL STAR? THE CHARACTERISTICS OF EXTREMELY METAL-POOR CARBON-RICH STARS

Takuma Suda,[1] Masayuki Aikawa,[1] Masahiro N. Machida,[2,3] and Masayuki Y. Fujimoto
Department of Physics, Hokkaido University, Sapporo 060-0810, Japan; suda@astro1.sci.hokudai.ac.jp, aikawa@nucl.sci.hokudai.ac.jp, machida@th.nao.ac.jp, fujimoto@astro1.sci.hokudai.ac.jp

and

Icko Iben, Jr.[4]
Departments of Astronomy and of Physics, University of Illinois at Urbana-Champaign, IL 61801; icko@astro.uiuc.edu
Received 2004 February 24; accepted 2004 April 22

ABSTRACT

We discuss the origin of HE 0107−5240, which, with a metallicity of $[Fe/H] = -5.3$, is the most iron-poor star yet observed. Its discovery has an important bearing on the question of the observability of first-generation stars in our universe. In common with other stars of very small metallicity ($-4 \lesssim [Fe/H] \lesssim -2.5$), HE 0107−5240 shows a peculiar abundance pattern, including large enhancements of C, N, and O, and a more modest enhancement of Na. The observed abundance pattern can be explained by nucleosynthesis and mass transfer in a first-generation binary star, which, after birth, accretes matter from a primordial cloud mixed with the ejectum of a supernova. We elaborate the binary scenario on the basis of our current understanding of the evolution and nucleosynthesis of extremely metal-poor, low-mass model stars and discuss the possibility of discriminating this scenario from others. In our picture, iron-peak elements arise in surface layers of the component stars by accretion of gas from the polluted primordial cloud, pollution occurring after the birth of the binary. To explain the observed C, N, O, and Na enhancements, as well as the $^{12}C/^{13}C$ ratio, we suppose that the currently observed star, once the secondary in a binary, accreted matter from a chemically evolved companion, which is now a white dwarf. To estimate the abundances in the matter transferred in the binary, we rely on the results of computations of model stars constructed with up-to-date input physics. Nucleosynthesis in a helium-flash–driven convective zone into which hydrogen has been injected is followed, allowing us to explain the origin in the primary of the observed O and Na enrichments and to discuss the abundances of *s*-process elements. From the observed abundances, we conclude that HE 0107−5240 has evolved from a wide binary (of initial separation ∼20 AU) with a primary of initial mass in the range 1.2–3 $M_\odot$. On the assumption that the system now consists of a white dwarf and a red giant, the present binary separation and period are estimated at ≃34 AU and a period of ≃150 yr, respectively. We also conclude that the abundance distribution of heavy *s*-process elements may hold the key to a satisfactory understanding of the origin of HE 0107−5240. An enhancement of $[Pb/Fe] \simeq 1$–2 should be observed if HE 0107−5240 is a second-generation star, formed from gas already polluted with iron-group elements. If the enhancement of main-line *s*-process elements is not detected, HE 0107−5240 may be a first-generation secondary in a binary system with a primary of mass less than 2.5 $M_\odot$, born from gas of primordial composition, produced in the big bang, and subsequently subjected to surface pollution by accretion of gas from the parent cloud metal-enriched by mixing with the ejectum of a supernova.

Subject headings: binaries: general — early universe — stars: abundances — stars: chemically peculiar — stars: individual (HE 0107−5240) — stars: Population II

1. INTRODUCTION

The discovery of the exceedingly metal-poor red giant HE 0107−5240 (Christlieb et al. 2002) has great importance for our understanding of early star formation in the Galaxy. It has the smallest metallicity ($[Fe/H] = -5.3$) of any star yet observed and it exhibits several abundance ratios that differ markedly from abundance ratios in solar system material. In particular, it shows large enhancements of carbon ($[C/Fe] = 4.0$), nitrogen ($[N/Fe] = 2.3$), and oxygen ($[O/Fe] = 2.4^{+0.2}_{-0.4}$) (Bessell et al. 2004), as well as a mild enhancement of sodium ($[Na/Fe] = 0.8$); currently, only an upper bound exists for the important *s*-process element Ba ($[Ba/Fe] < 0.8$) (Christlieb et al. 2002). We use the traditional term "metal-poor" in referring to HE 0107−5240 even though, thanks to the large abundances of CNO elements relative to Fe, it is certainly not "heavy-element–poor."

Recent papers that discuss the origin of HE 0107−5240 use arguments involving supernova nucleosynthesis in a primordial cloud (Umeda & Nomoto 2003; Limongi et al. 2003), external pollution after birth (Shigeyama et al. 2003), and the mass distribution predicted by theories of star formation (Schneider et al. 2003; Omukai & Yoshii 2003). Shigeyama et al. (2003) predict a metallicity distribution function for first-generation (Population III) stars currently burning hydrogen and conclude that HE 0107−5240 is a first-generation object with a surface affected by accreting interstellar matter polluted with heavy elements. Umeda & Nomoto (2003) adjust

[1] Meme Media Laboratory, Hokkaido University.
[2] Current address: Center for Frontier Science, Chiba University, Yayoicho 1-33, Inageku, Chiba, 263-8522, Japan.
[3] National Astronomical Observatory of Japan, Mitaka, Tokyo, 181-8588, Japan.
[4] Visiting JSPS Eminent Professor, Hokkaido University.

parameters in a first-generation supernova model in such a way as to produce a C/Fe ratio in the supernova ejectum that agrees with the ratio observed in HE 0107−5240 and argue that HE 0107−5240 is a second-generation object formed from the primordial cloud after it has been mixed with the ejectum of the supernova. A similar scenario is presented by Limongi et al. (2003), who argue that the HE 0107−5240 abundances can be produced by a combination of two types of supernova ejecta: a normal ejectum consisting of $\sim 0.06\ M_{\odot}$ of iron, and an abnormal ejectum consisting only of products of partial helium burning. Although all extant scenarios address important aspects of the problem, further discussion is warranted of the physics of star formation and of the chemical composition expected in a primordial cloud into which matter ejected by a supernova has been mixed. More importantly, the modifications of surface abundances that HE 0107−5240 has suffered during its long life should be elucidated. In particular, the possibility of accretion from an evolved first-generation companion that has mixed to its surface products of internal nucleosynthesis should be explored. In this paper we describe results of such an exploration.

A major characteristic of models of extremely metal-poor stars is that, although the *p-p* chain reactions are the dominant source of the stellar luminosity and the main driver of evolution during most of the core hydrogen-burning phase, the CNO cycles play an increasingly important role as evolution progresses beyond the main-sequence phase. This is because, as temperatures increase, carbon is produced by the highly temperature-sensitive 3α reaction and because, at high temperatures, only a small abundance of CNO elements is needed for CNO cycle reactions to become the dominant driver of evolution. This characteristic behavior of the evolution of zero-metallicity stars has been explored by many authors, from the early works of Wagner (1974), D'Antona (1982) and Guenther & Demarque (1983) through more recent works restricted to the low- and intermediate-mass stars of concern here (Weiss et al. 2000; Marigo et al. 2001; Chieffi et al. 2001; Schlattl et al. 2001, 2002; Siess et al. 2002). In particular, Fujimoto et al. (1990, 2000) and Hollowell et al. (1990) have shown that low- and intermediate-mass stars follow evolutionary trajectories significantly different from those followed by Population I and Population II stars, becoming carbon stars at a much earlier stage.

Since the early 1990s, the nature of the evolution of metal-poor stars has been illuminated considerably by the observations. Studies of the abundance patterns found in stellar spectra have revealed that carbon stars are not rare among metal-poor stars and that the relative frequency of such stars increases with decreasing metallicity, amounting to more than $\sim$20% for stars with $[\mathrm{Fe/H}] \lesssim -2.5$ (Rossi et al. 1998). It has been known for a long time that most Population I carbon stars that are not evolved beyond the first red giant branch (RGB) are in binaries with a white dwarf companion (McClure et al. 1980); this is also true of Population II CH stars (McClure 1984). Thus, the frequency of carbon stars among low-metallicity stars may suggest a high rate of binary star formation in the gas clouds out of which such stars were formed. A current lack of evidence for radial velocity variations does not necessarily rule out the possibility that the observed star is now in a very wide binary or that the initial binary was disrupted at some point after the mass-transfer episode occurred. Since an initial binary must be wide enough to accommodate an asymptotic giant branch (AGB) star that does not overflow its Roche lobe, and since, if anything, the binary becomes wider as the AGB star loses mass (see, e.g., the discussion in Iben 2000), it is probable that the binary separation does not decrease. Furthermore, given the fact that wide binaries are relatively easily disrupted in close stellar encounters (Heggie 1975), it may happen that, in 10^{10} yr of traveling through the Galaxy, HE 0107−5240 has lost a one-time companion. The radial velocity of HE 0107−5240 has recently been determined to be 44.5 ± 0.5 km s^{-1}, based on observations over a 373 day time span (Bessell et al. 2004). Although significant radial velocity variations have not been detected, observations over a much longer baseline would be well worth undertaking.

Extremely metal-poor stars show a large dispersion in the abundance ratios among metals. The fact that, for metallicities less than $[\mathrm{Fe/H}] \simeq -2.5$, this dispersion increases with decreasing metallicity may be interpreted to mean that these stars were born from interstellar gas that was polluted by a small number of supernovae, so that stellar abundances reflect intrinsic variations in the yields of those individual supernovae that contribute to the pollution of the gas.

The abundances of many neutron-rich elements vary considerably from star to star even among those stars that have the abundance ratio [Ba/ Eu] very close to the solar *r*-process value (McWilliam 1998; Aoki et al. 2002a; Honda et al. 2004). This fact has been used to argue that the Ba found in the spectra of stars of low metallicity has been created by an *r*-process mechanism in supernovae and that the production rate varies considerably from one supernova to another (McWilliam 1998). However, there are also large variations from one star to another in the abundances of those neutron-rich elements that are unquestionably made by the *s*-process (see, e.g., Aoki et al. 2001; Ryan et al. 2003 and references therein). It is known that thermally pulsing AGB stars are the most likely sites for the formation of heavy *s*-process elements. Since most extremely metal-poor stars are not AGB stars, it seems plausible to invoke the erstwhile presence of an initially more massive binary companion that has produced the *s*-process elements, dredged these elements to the surface, and then transferred enriched matter to the less evolved component, a scenario suggested by Fujimoto et al. (2000) and explored by Goriely & Siess (2001), Aoki et al. (2001), and Iwamoto et al. (2004). These authors point out that *s*-process nucleosynthesis in very metal-poor stars may differ significantly from that which is thought to operate in younger populations.

The purpose of the present paper is to review the possible scenarios for explaining the observed properties of HE 0107−5240 and to investigate the possibility of discriminating among these scenarios on the basis of our current understanding of nucleosynthesis in extremely metal-poor stars—an understanding that has been achieved by comparing results of theoretical evolutionary calculations with the observations. In the following, we define stars of metallicity less than $[\mathrm{Fe/H}] \lesssim -2.5$ as "extremely metal-poor" (EMP) stars and examine the implications of assuming that HE 0107−5240 was born as a single star or as a low-mass component in a binary system. We use the results of new evolutionary models of Population III stars of mass in the range 0.8–4 $M_{\odot}$ to elaborate the binary scenario more fully. Stellar model construction employs up-to-date input physics (Suda 2003) that differs in significant ways from the input physics employed by Fujimoto et al. (1990, 2000), and the results, correspondingly, differ quantitatively in significant ways. In addition, we rely upon new results concerning neutron-capture nucleosynthesis in a helium-flash–driven convection zone that is a consequence of the ingestion of protons into this convection zone (M. Aikawa et al. 2004, in preparation).

In discussing the origin of HE 0107−5240, it is important to consider separately (1) the source of iron group elements, (2) the source of light elements such as the α-rich elements C and O and the secondary elements N and Na, and (3) the source of *s*-process elements. The two possibilities for explaining the metals are (1) accretion of metal-rich gas by a first-generation (Population III) star and (2) formation as a second-generation star out of matter in which metals are present in consequence of mixing with the ejectum of a first-generation supernova. In the binary scenario, the enhancements of CNO elements and of *s*-process elements are assumed to be due to accretion from an AGB companion that has experienced one or more dredge-up episodes that bring to the surface the result of nucleosynthesis and mixing in its interior.

There is not yet a consensus as to the conditions that are necessary for the formation of low-metallicity, low-mass stars. The lack of a sufficient abundance of metals to provide a straightforward and effective cooling mechanism for metallicities $[\mathrm{Fe/H}] \lesssim -4$ (Yoshii & Sabano 1980; see also Omukai 2000) is the primary hurdle facing low-mass star formation in the early universe. In the absence of metals, the hydrogen molecule can produce cooling, but estimates of the minimum Jean's mass vary from $\sim$1 (Sabano & Yoshii 1977) and $\sim$0.1 $M_\odot$ (Palla et al. 1983) to $\gtrsim$60 $M_\odot$ (Yoneyama 1972). Several authors argue that low-mass stars can form from a metal-free primordial gas cloud (e.g., Rees 1976; see also Uehara et al. 1996), whereas others suggest that only massive stars can form from such a cloud (e.g., Omukai & Nishi 1998; Bromm et al. 1999). To complicate the picture even further, two-dimensional hydrodynamical simulations (Nakamura & Umemura 2001, 2002) suggest a bimodal initial mass function for Population III stars. Such complexity may arise from the fact that, in primordial clouds of mass $\sim 10^6$ $M_\odot$ that first collapse (e.g., Tegmark et al. 1997), the scarcity of free electrons (mole density $\sim 10^{-4}$; Galli & Palla 1998) limits the formation of H_2 molecules that can act as cooling agents. On the other hand, if the cloud temperature is raised above 10^4 K and gas is reionized, the ionization fraction remains quite high during the subsequent radiative cooling phase and increases the abundances of H_2 and HD sufficiently to allow the birth of low-mass stars even in the complete absence of metals (Shapiro & Kang 1987; see Uehara & Inutsuka 2000 for a recent computation including HD molecules). This may be the case for primordial clouds as massive as $\gtrsim 10^8$ $M_\odot$ for which virial temperatures are larger than 10^4 K, although the collapse is delayed somewhat compared with the case of less massive clouds (see e.g., Nishi & Susa 1999). The same situation also prevails even for less massive primordial clouds when the interstellar gas is swept up and heated by the supernova shock produced by a first-generation massive star (Machida et al. 2004). It is also argued that low-mass star formation is possible in clouds of the primordial composition if matter is irradiated by sufficiently strong far-UV radiation from first-generation massive stars (Haiman et al. 1996b; Omukai & Yoshii 2003). If the observed enrichment of CNO elements can be explained as acquired after birth, the very existence of HE 0107−5240 indicates that some of these or other formation mechanisms of low-mass stars have to work even in the gas clouds completely devoid of metals.

Observationally, there has been long, continuous interest in search for stars of lower metallicity and/or completely devoid of metals since the first discovery of stars of 1/10–1/100 solar metallicity in the 1950s (Chamberlain & Aller 1951). At the beginning of the 1970s, a survey up to a limiting magnitude of $B \simeq 11.5$ (Bond 1970) found no star with $[\mathrm{Fe/H}] < -3$ (Bond 1980, 1981) and encouraged the idea that no star of metallicity smaller than this had been formed in our universe. In the early 1980s, however, as by-products of the study of high-velocity stars and blue subdwarfs, the dwarf G64-12 with $[\mathrm{Fe/H}] = -3.5$ (Carney & Peterson 1981) and the giant CD $-38^\circ 245$ with $[\mathrm{Fe/H}] = -4.5$ (Bessell & Norris 1984) were found, at magnitudes, respectively, of $B = 11.8$ and $B = 12.0$, both below the limiting magnitude of the survey by Bond (1970). In the early 1990s, the HK survey (Beers et al. 1985, 1992), with a limiting magnitude of $B = 15.5$, uncovered over 100 stars with $[\mathrm{Fe/H}] < -3$, and, yet, it found no star with $[\mathrm{Fe/H}] < -4.0$. As an aside, we note that the metallicity of CD $-38^\circ 245$ has been revised upward to $[\mathrm{Fe/H}] = -3.92$ (Ryan et al. 1996). Some time ago, a high-velocity carbon dwarf G77-61, at $B = 15.60$ ($V = 13.90$), was assigned a metallicity of $[\mathrm{Fe/H}] = -5.6$ (Gass et al. 1988); however, the low surface temperature of the star and the presence of crowded molecular lines makes the abundance analysis very difficult, and further work is required to confirm the early estimate of metallicity. Finally, the Hamburg/ESO survey, with a limiting magnitude of $B = 17.5$ (Christlieb et al. 1999), discovered HE 0107−5240 with metallicity $[\mathrm{Fe/H}] = -5.3$ at magnitude $B = 15.89$. Along with the increase in the limiting magnitude, therefore, we have been able to detect the stars of smaller metallicity. Provided that the sample of stars of metallicity as small as, and still smaller than, that of HE 0107−5240 can be considerably augmented, the discovery of HE 0107−5240 may be the beginning of a new epoch in the study of the early history of the universe using low-mass stellar survivors as a tool.

The paper is organized as follows: In § 2 formation scenarios are discussed. In § 3 the characteristics of evolution and nucleosynthesis in low- and intermediate-mass metal-free and metal-poor stars are reviewed and compared with the results of recent observations of extremely metal-poor stars. In § 4 the origin of HE 0107−5240 is discussed and the binary scenario is elaborated. Conclusions and further discussion are provided in § 5.

2. POSSIBLE FORMATION SCENARIOS OF HE 0107−5240

The origin of metals in HE 0107−5240 must be the consequence of pollution. It is reasonable to suppose that the low-mass star currently observed was formed in a primordial cloud composed initially of matter in the abundance distribution produced by the big bang. If it was born before, or simultaneously with, the progenitor of the first supernova that occurred in this cloud, we refer to it hereafter as a first-generation (Population III) star; after birth, it may have accreted matter polluted by the ejectum of the first supernova. If it was born after the first supernova occurred in the cloud, we refer to it hereafter as a second-generation star; the matter out of which it was formed was already polluted by the ejectum of a supernova and subsequent accretion from the polluted cloud would not significantly alter the surface abundances of the star. In either case, while traveling for 10^{10} yr through our Galaxy, the currently observed star must have continued to accrete matter from the Galactic interstellar medium. Thus, there are at least three distinct possibilities for explaining the observed metallicity: (1) a first-generation star that accretes polluted material in a primordial cloud, (2) a second-generation star formed in a primordial cloud, and (3) a first- or second-generation star that acquires most of its metals by accretion from the Galactic interstellar medium.

We examine first the (third) possibility that accretion from interstellar gas clouds composed of matter with abundances in Population I and Population II distributions could by itself have produced the surface abundances in HE 0107−5240. For an order of magnitude estimate of the accretion rate $\dot{M}$, we adopt the gravitational focusing cross section (Hoyle & Lyttleton 1939)

$$\sigma_{\rm acc} = \pi b_{\rm crit}^2, \tag{1}$$

where the critical impact parameter is given by

$$b_{\rm crit} = \frac{2GM}{v^2}. \tag{2}$$

In this equation, G is the gravitational constant, M is the mass of the star, and v is the velocity of the star relative to the velocity of the gas cloud through which it is passing. Calling n the average number density in a cloud, assumed to be of uniform density and temperature throughout, and calling μm_a the average mass of a cloud particle, where m_a is the atomic mass unit and μ is a number of the order of unity, the mass accretion rate is

$$\dot{M}_{\rm acc} = n\mu m_a \sigma_{\rm acc} v \tag{3}$$

$$= 5.9\times10^{-12}\mu\left(\frac{n}{\rm cm^{-3}}\right)\left(\frac{M}{M_\odot}\right)^2\left(\frac{\rm km\ s^{-1}}{v}\right)^3 M_\odot\ {\rm yr}^{-1}. \tag{4}$$

Bondi & Hoyle (1944) arrive at a value smaller than this by a factor of 2.5/4. Bondi (1952) replaces v in equation (2) by $\left(v^2 + c_s^2\right)^{1/2}$, where c_s is the average speed of sound in a cloud, basically to avoid a formal divergence when v vanishes. Given that no version of the simple accretion formula is other than a crude approximation, and given the fact that we can make only order of magnitude estimates of n and v, we settle on

$$\dot{M}_{\rm acc} = 4\times10^{-18}\ nM_*^2 v_{100}^{-3}\ M_\odot\ {\rm yr}^{-1}, \tag{5}$$

where n is the particle density in cm^{-3}, M_* is the mass of the star in solar units, and v_{100} is the relative velocity in units of 100 km s^{-1}.

The typical space velocity of a low-metallicity star is now of the order of 100 km s^{-1}, and this should not have changed appreciably over the last 10^{10} yr. If, in the primordial Galaxy, $10^{11}\ M_\odot$ of baryonic matter were distributed uniformly in a sphere of radius 10 kpc, the particle density would be of the order of $n \sim 1$ cm^{-3}. If the gas in the disk of the current Galaxy is of mass $\sim10^9\ M_\odot$ and if the disk is of thickness 200 pc and radius 10 kpc, the mean density is also ~1 cm^{-3}. We therefore assume that, over a time T and path length $l = \int_0^T dl$, the average density of matter encountered by a star is $\bar{n} = \int_0^T n dl/l \sim 1$ cm^{-3}. From equation (5), we estimate that, over a time $T = 10^{10}$ yr, an $0.8\ M_\odot$ star accretes a mass of about $2.6\times10^{-8}\ M_\odot$. Generously assuming that the metallicity of matter in the average cloud encountered is solar, and adopting $0.2\ M_\odot$ as the mass of the convective envelope in a metal-poor red giant, we obtain $[{\rm Fe/H}] \simeq -6.7 + 2\log M_*$ for the surface metallicity after the primordial star has become a red giant, far too small to account for HE 0107−5240. Adopting $[{\rm Fe/H}] \simeq -1$ as a more reasonable choice for the average metallicity of accreted matter, an average particle density larger than $\sim200/M_*^2$ cm^{-3} is required to reproduce the metallicity of HE 0107−5240. Thus, accretion from interstellar matter during oscillations back and forth in the Galaxy does not appear as a very promising explanation for the metallicity of any metal-poor star, let alone HE 0107−5240.

We examine next the first possibility: birth of a first-generation low-mass star (possibly in a binary) in a primordial cloud before it has been polluted, and subsequent accretion of matter in the cloud that has been mixed with the ejecta of supernovae. In the current bottom-up scenarios of structure formation such as cold dark matter models, the first collapsed objects should have mass scales of $\sim10^6\ M_\odot$ (e.g., Haiman et al. 1996a; Tegmark et al. 1997), in which baryons contribute ~10% of the matter. If we assume $v \approx 10$ km s^{-1} and $n \approx 10$ cm^{-3}, equation (5) gives

$$\dot{M}_{\rm acc} = 4\times10^{-14}\ n_{10}M_*^2 v_{10}^{-3}\ M_\odot\ {\rm yr}^{-1}, \tag{6}$$

where n_{10} is the number density in units of 10 cm^{-3} and v_{10} is the relative velocity in units of 10 km s^{-1}. When mixed with the ejectum of a first supernova (assuming the mass yield of iron group elements to be $M_{\rm Fe} = 0.1 \sim 1\ M_\odot$), the metallicity of the first collapsed cloud becomes $[{\rm Fe/H}] = -3 \sim -2$; this, of course, increases as more supernovae occur. If the accreting star remains in the cloud for $T \sim 10^9$ yr, it accretes a mass of $M_{\rm acc} \sim 10^{-4}\ M_\odot$, which is several thousand times larger than the mass it is expected to accrete from the Galactic interstellar medium after the primordial cloud has mixed (dissolved) into the Galaxy. If the time-averaged metallicity of the cloud is $[{\rm Fe/H}] \simeq -2$, then, when the accreting star becomes a red giant with a convective envelope of mass $\sim0.2\ M_\odot$, the surface metallicity of the star reproduces that of HE 0107−5240.

We examine finally the second possibility: a second-generation star born from gas that has been polluted by the mixing of primordial matter with the ejectum of a first-generation supernova. As the shock wave produced by a supernova sweeps through the cloud, gas is compressed into a shell in which possibly low-mass stars can form (Machida et al. 2004). Estimating $\sim10^5\ M_\odot$ as the mass of intracloud gas that is swept up in the primordial cloud and adopting a nucleosynthetic yield of $M_{\rm Fe} = 0.1 \sim 1\ M_\odot$ for Type II supernovae, an average value of $[{\rm Fe/H}] = -3 \sim -2$ can be estimated for second-generation stars. In this scenario, the large dispersion in the surface abundance ratios of metals among metal-poor stars of metallicity around $[{\rm Fe/H}] \lesssim -2.5$, found by the HK survey (Beers et al. 1992), may be attributed to a dispersion in the abundance distribution produced by individual supernovae. However, in this standard scenario, stars with metallicity as small as that of HE 0107−5240 are not likely to be formed. Accordingly, only if the supernona ejectum is diluted somehow in a primordial condensation more massive than $\sim10^7\ M_\odot$ (in baryonic mass), can the desired metallicity be achieved. It is true that low-luminosity supernovae are observed with an Fe yield ~100 times less than that of a typical supernova, but it is hard to trigger star formation since, because of low energy, the supernova shock is dissolved before initiating the fragmentation in the swept-up gas shell (Machida et al. 2004).

In closing this section, we comment on the scenario for the formation of HE 0107−5240 proposed by Umeda & Nomoto (2003). They show that, except for the abundance of nitrogen and sodium, the observed element abundances of HE 0107−5240 can be explained by assuming that the star was born out of matter produced by mixing the ejectum of an unusual Type II supernova with a judiciously chosen mass of primordial

matter. They argue that the nitrogen not produced by the supernova model appears at the surface of the present star in consequence of a first dredge-up episode on the RGB. As will be discussed in § 4, we have calculated the evolution of a model star of mass 0.8 $M_{\odot}$ and of a chemical composition suggested by Umeda & Nomoto (2003) and find that, indeed, the [N/Fe] ratio in HE 0107−5240 can be reproduced during the first dredge-up episode. Thus, one important aspect of the Umeda-Nomoto scenario is confirmed. However, the enrichment of Na has yet to be explained. In addition, when we consider the likelihood of the formation of a low-mass star from the polluted cloud postulated by Umeda & Nomoto (2003), several problems arise. The mass of carbon ejected by the postulated supernova is $M_{\rm C} \simeq 0.2\ M_{\odot}$, implying that the mass of primordial matter mixed with the ejectum is only

$$M_{\rm shell} = \frac{M_{\rm C}}{X_{\rm C,\odot} \times 10^{\rm [C/H]}} \approx 1.3 \times 10^{3}\ M_{\odot}, \qquad (7)$$

where $X_{\rm C,\odot} = 3.0 \times 10^{-3}$ is the solar abundance by mass of carbon and $\rm [C/H] = -1.3$ is the carbon abundance in HE 0107−5240. This is a factor of ∼100 smaller than the mass that must be swept up into a gas shell by a first-generation supernova before fragmentation is expected to occur in the shell (Machida et al. 2004). Thus, star formation in the swept-up gas shell is unlikely. If, despite these arguments, star formation can occur within such a small shell, one might anticipate that pollution by normal supernovae with similar or larger mass yields of iron group elements would give rise to the formation of stars of metallicity $\rm [Fe/H] \gtrsim -1$. This, however, leads to difficulty in explaining the origin of extremely metal-poor stars of metallicity $\rm [Fe/H] \simeq -3$.

In summary, the viable scenarios for the formation of HE 0107−5240 are the following:

1. A first-generation star that

a) disguises its surface by accreting metals in the parent primordial cloud polluted by the ejectum of a normal supernova and then

b) accretes, from an evolved companion in a binary system, matter containing CNO and *s*-process elements produced in the interior of the companion.

2. A second-generation star that

a) forms in a primordial cloud of total (dark matter plus baryonic matter) mass $\gtrsim 10^{8}\ M_{\odot}$ polluted by the ejectum of a normal supernova and acquires CNO elements from an evolved binary companion, or

b) forms from material polluted by the ejectum of a very unusual supernova that makes C, O, and Na in the currently observed ratios.

In the following, we examine how one may choose from among these scenarios by using knowledge gained from a study of the evolution of metal-free and metal-poor model stars.

3. EVOLUTIONARY CHARACTERISTICS OF LOW- AND INTERMEDIATE-MASS METAL-POOR STARS

Many numerical computations of the evolution of low- and intermediate-mass Population III and EMP stars and discussions of their characteristics have been published (Wagner 1974; D'Antona 1982; Guenther & Demarque 1983; Fujimoto et al. 1990, 1995, 2000; Hollowell et al. 1990; Cassisi & Castellani 1993; Cassisi et al. 1996; Weiss et al. 2000; Marigo et al. 2001; Chieffi et al. 2001; Schlattl et al. 2001, 2002; Siess et al. 2002). It is commonly accepted that, as first shown by Fujimoto et al. (1990), a carbon enhancement occurs at the core helium flash stage in low-mass model stars. Evolutionary destinations are illustrated by Figure 2 of Fujimoto et al. 2000; hereafter FII00) as a function of initial metallicity and mass. Although some differences in the evolution of low-mass Population III stars are reported by other groups (Schlattl et al. 2002; Siess et al. 2002), qualitative results are not different from those found by FII00.

Nevertheless, because there are many important aspects of nucleosynthesis that have not yet been adequately addressed, we have computed additional models of zero-metallicity stars of mass ranging from 0.8 to 4.0 $M_{\odot}$. We have used the stellar evolution code employed by FII00 (see e.g. Iben et al. 1992), modified with up-to-date input physics (Suda 2003); radiative opacities are taken from OPAL tables (Iglesias & Rogers 1996) and Alexander & Ferguson (1994) tables, complemented in regions not covered by the tables by analytic approximations (Iben 1975). Itoh et al. (1983) is adopted for electron conductivity in dense regions of the stellar interior; elsewhere, conductive opacities are calculated with a fitting formula (Iben 1975) based on Hubbard & Lampe (1969) (for details of interpolation, see Suda 2003). Neutrino loss rates are taken from fitting formulae by Itoh et al. (1996). The NACRE compilation (Angulo et al. 1999) is used for nuclear reaction rates involving proton, α, and electron capture for ^{1}H, ^{3}He, ^{4}He, ^{12}C, ^{14}N, ^{16}O, ^{18}O, ^{22}Ne, and ^{25}Mg. In treating convection, we adopt the standard mixing-length formulation, choosing the parameter $\alpha = 1.5$, and use the Schwarzschild criterion for instability against convection.

For models of initial mass $M \leq 1.1\ M_{\odot}$, the star reaches the RGB with an electron-degenerate helium core before helium ignites off-center in the core and forces the development of a convective shell. The entropy barrier between the helium convective region and the hydrogen-rich envelope is small. Thus, as it extends outward, the outer edge of the convective region generated by the off-center helium core flash penetrates the hydrogen profile. Hydrogen is mixed into the convective shell and a hydrogen-shell flash is ignited. The initial convective region splits into two convective zones, the inner one driven by the helium core flash and the outer one by the hydrogen shell flash. The convection zone sustained by hydrogen burning extends outward, adding fuel by ingesting protons. These developments are qualitatively consistent with FII00, although quantitative results are different. The expansion of the hydrogen-flash–driven convection zone brings about the movement inward in mass of the base of the surface convective zone and the dredge-up of nuclear matter processed in the hydrogen mixed region, changing the surface chemical composition dramatically. Hereafter, we refer to these processes, triggered by hydrogen mixing into a helium-flash–driven convective zone, as He-FDDM (helium-flash–driven deep mixing).

For $M \geq 1.2\ M_{\odot}$, helium ignites at the center before electron degeneracy has set in, and the model avoids the RGB configuration (stable hydrogen-burning in a shell above an electron-degenerate helium core). After helium is exhausted at the center, the star adopts an early asymptotic giant branch (EAGB) configuration consisting of an electron-degenerate carbon-oxygen (CO) core capped by a helium-rich shell (at the base of which helium is initially burning) and a hydrogen-rich envelope (at the base of which hydrogen is not initially burning). Almost immediately the models evolve into thermally pulsing AGB (TPAGB) stars with nuclear energy being produced

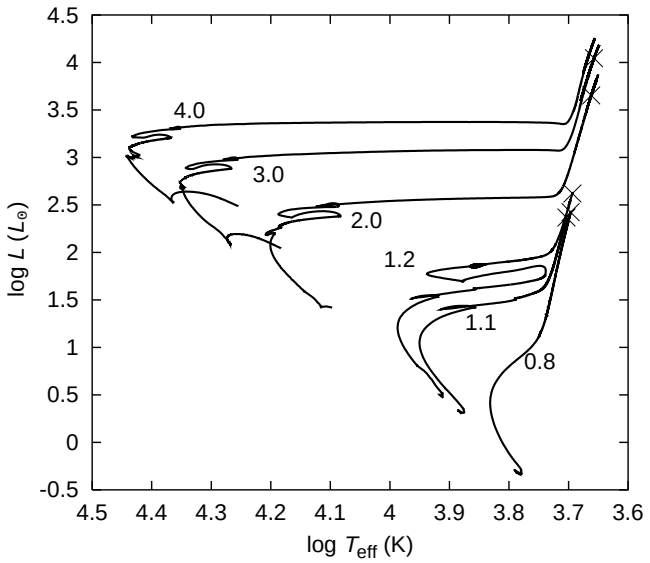

FIG. 1.—Evolutionary trajectories of Population III model stars in the H-R diagram. Numbers beside each curve denote the model mass, M, in units of the solar mass. For model stars of mass $M \leq 3\ M_{\odot}$, evolution is followed from the zero-age main sequence through the stage when the helium-flash–driven convective zone engulfs hydrogen and initiates the helium-flash–driven deep mixing (He-FDDM) mechanism. Evolution of the model of mass 4 $M_{\odot}$ is terminated along the TPAGB branch when thermal pulses reach an asymptotic strength. Crosses mark where the He-FDDM event begins, on the RGB for models of mass $M \leq 1.1\ M_{\odot}$ or at the beginning of the TPAGB for models of mass $M \geq 1.2\ M_{\odot}$.

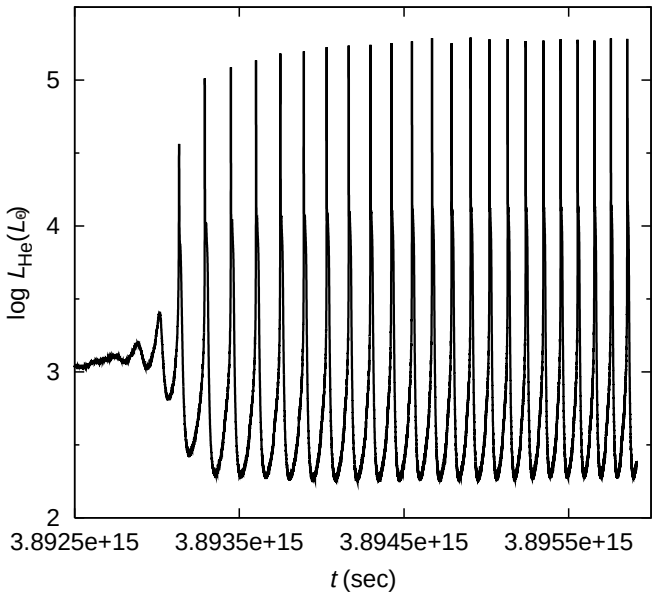

FIG. 2.—Variations in the helium-burning luminosity during the TPAGB phase for a Population III star of mass 4 $M_{\odot}$.

alternately by helium burning and hydrogen burning. For models of mass $1.2\ M_{\odot} \leq M \leq 3\ M_{\odot}$, a He-FDDM episode initiates the TPAGB phase when the first helium convective region touches the hydrogen profile. The subsequent ingestion of hydrogen into the helium convective zone and the formation of two convective zones followed by dredge-up of nuclearly processed material into the envelope is expected to proceed just as in the case of low-mass models that ignite helium under electron-degenerate conditions. The He-FDDM episode does not occur in the $M = 4\ M_{\odot}$ model.

The duration of the He-FDDM event is so short that our treatment of convective mixing is not correct, so, in both the RGB and AGB cases, we have terminated our computations at the start of this event. A correct time-dependent study of He-FDDM has been conducted by Hollowell et al. (1990), and we assume that the qualitative behavior of all such events is essentially invariant. Details of the evolution after the mixing episode will be provided in a subsequent paper (T. Suda, M. S. Fujimoto, & I. Iben 2004, in preparation).

Figure 1 shows a selection of evolutionary tracks of Population III models in the H-R diagram. For stars of $M \leq 3.0\ M_{\odot}$, evolution is terminated at the point when models begin the He-FDDM episode that turns them into carbon stars. Compared with Population I and Population II model stars, Population III model stars become carbon stars at significantly smaller luminosities, and hence, smaller radii.

Recently, Chieffi et al. (2001) and Siess et al. (2002) have computed the evolution of Population III stars of mass $M \geq 4\ M_{\odot}$, forcing mixing across the boundary between the carbon-rich helium layer and the hydrogen-rich layer that is formed when the outer edge of the convective zone engendered by helium burning approaches the hydrogen-rich layer. They contend that this "carbon injection" mechanism is different from the He-FDDM mechanism and is caused by convective overshoot. Because of a huge jump in the carbon abundance across the boundary, by many orders of magnitude, the mixing of carbon into the hydrogen-rich layer enormously enhances the hydrogen-burning rate, giving rise to an "irreversible" process (Siess et al. 2002). The initial increase in the surface carbon abundance leads to full amplitude thermal pulses and third dredge-up episodes similar to those in Population I and II stars, resulting in surface enhancements of C, N, and O similar to those observed in HE 0107−5240; the oxygen enhancement is due to the reaction $^{12}\mathrm{C}(\alpha,\gamma)^{16}\mathrm{O}$ at high temperatures (see the discussion in § 3.3). These results, however, may depend critically on the adopted assumptions, and in particular, may be an artifact of the adopted prescription for convective overshoot.

We compute the evolution of a 4 $M_{\odot}$ star without any special treatment of convective overshooting. In addition, we treat changes in chemical composition explicitly, with small time steps, so as to maintain consistency with the associated energy-generation rates; the difference in the changes in chemical composition may affect the temperature structure in the helium core through compression. Figure 2 shows the resultant variations in the helium-burning luminosity. We confirm that thermal pulses do occur, in agreement with Siess et al. (2002), but in disagreement with results of earlier computations (Chieffi & Tornambé 1984) and of a related semianalytical study (Fujimoto et al. 1984). These discrepancies must be due to the sensitivity of results to the input physics.

The TPAGB evolution of our 4 $M_{\odot}$ model star starts when the core mass is $M_c = 0.873\ M_{\odot}$, and we have followed 23 thermal pulses until a locally asymptotic strength (Fujimoto & Sugimoto 1979) of $L_{\mathrm{He}}^{\mathrm{max}} = 1.9 \times 10^5\ L_{\odot}$ is reached. In contrast with the Seiss et al. calculations, we do not find any direct mixing between the carbon-rich and hydrogen-rich layer. The minimum distance between the outer edge of the helium-flash–driven convective zone and the base of the hydrogen profile is always larger than a pressure scale height ($\sim 1.4 H_P$).

Further investigations are necessary to determine the relevance of intermediate-mass metal-poor models to HE 0107−5240, as well as to determine why, in contrast with such models constructed two decades ago, current models experience thermal pulses.

3.1. C *and* N *Enhancements*

As described in the evolutionary diagram in FII00, and consistent with the results we have obtained here, the evolution of low- and intermediate-mass stars may be classified into the following groups. For $M \leq 1.1\ M_{\odot}$ and $[\mathrm{Fe/H}] \lesssim -4.5$ (case I; FII00), the model becomes an RGB star before experiencing the He-FDDM mechanism; For $M \leq 1.1\ M_{\odot}$ and $-4.5 \lesssim [\mathrm{Fe/H}] \lesssim -2.5$ (case II), a model experiences the He-FDDM at the start of the TPAGB phase. If stellar mass is in the range $1.2 \leq M/M_{\odot} \lesssim 3$ and $[\mathrm{Fe/H}] \lesssim -2.5$ (case II′), models undergo the He-FDDM during the EAGB phase. As a consequence of the dredge-up of matter that has been processed by helium burning and then processed by proton capture reactions, metal-poor stars become nitrogen-rich carbon stars. In particular, low-mass stars of the case I and case II varieties increase their surface carbon and nitrogen abundances to the extent that $[\mathrm{C+N/H}] = 0 \sim -1$ during a single He-FDDM mixing episode, with $\mathrm{C/N} \simeq 1 \sim 1/5$ for case I and case II, respectively (Hollowell et al. 1990; Fujimoto et al. 2000; Schlattl et al. 2002). In case II models, the abundance ratio of C to N in the hydrogen flash convective zone is larger than in case I models since, owing to a larger mass, and hence, a deeper gravitational potential of the core, more helium has to be burned (yielding a larger C abundance) before the outer edge of the helium convective zone reaches the base of the hydrogen-rich layer. In case II′ models, on the other hand, the enhancement of C and N due to the He-FDDM event is relatively small since (1) the mass of the helium convective zone, and hence, the amount of C- and N-rich matter dredged up, decreases with increasing core mass, and (2) the dilution in the envelope increases with increasing envelope mass. After the surface abundance is increased above $[\mathrm{CNO/H}] \simeq -2.5$, the model stars behave similarly to those with metallicity $[\mathrm{Fe/H}] \gtrsim -2.5$. This is because the structure of the hydrogen-burning shell during the TPAGB stage is controlled mainly by the hydrogen shell burning rate that depends only on the CNO abundance; the opacity in the shell is dominated by electron scattering and therefore depends very little on the metallicity. Accordingly, the helium-flash convective zone cannot reach the base of the hydrogen-rich shell, and the He-FDDM mechanism does not occur. The models enter the TPAGB evolutionary phase in the same fashion as do model stars of younger populations (FII00); successive third dredge-up episodes increase the surface C abundance and lead to a large C/N abundance ratio.

3.2. *Neutron Capture Nucleosynthesis*

The character of mixing during a He-FDDM event, as studied in detail by Hollowell et al. (1990), is illustrated schematically in Figure 3*a*. As the helium shell flash develops, the helium convective zone grows in mass until, near the peak of the flash, its outer edge extends into the hydrogen-rich layer. Hydrogen is then carried downward by convection until it reaches a point where the lifetime of a proton becomes less than the convective mixing timescale; at this point, hydrogen burns via the $^{12}\mathrm{C}(p,\gamma)^{13}\mathrm{N}$ reaction. With the additional energy flux produced by this burning reaction, the shell convective zone splits into two parts, the outer one driven by the energy flux due to hydrogen burning and the inner one driven by the energy flux due to helium burning. The convective shell engendered by hydrogen burning transports C- and N-rich matter outward, where it can ultimately be incorporated into the envelope convective zone. In models with large core masses, the convective shell sustained by helium burning persists even after the hydrogen-driven convective zone has disappeared (FII00; Iwamoto et al. 2004).

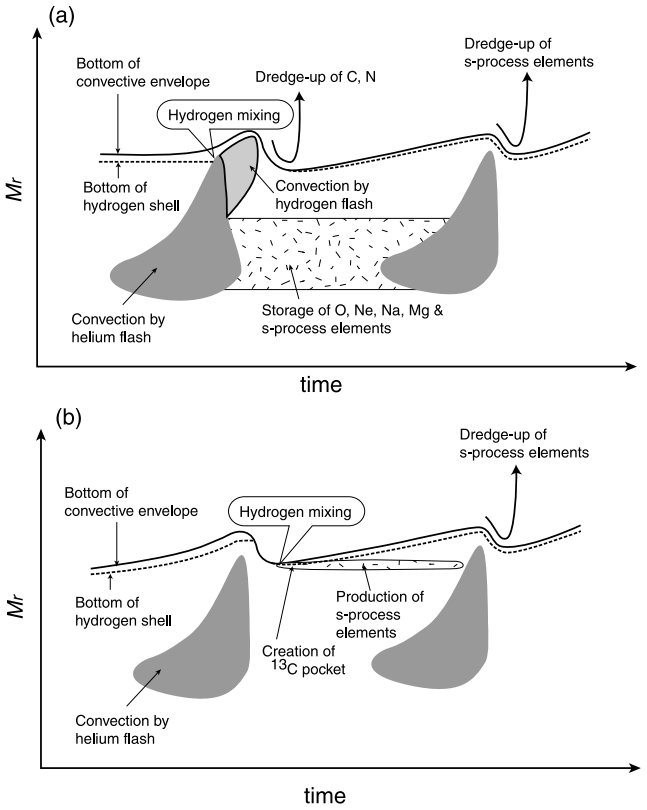

FIG. 3.—Schematic representations of the time dependence of (1) convective zones associated with helium-shell flashes and (2) sites for the nucleosynthesis and/or storage of *s*-process elements associated with these flashes. Panel (*a*) describes characteristics of the convective ^{13}C-burning model associated with a He-FDDM episode. The phenomenon begins when hydrogen is ingested by a convective zone driven by the energy flux from a unique helium-burning flash in an EMP ($[\mathrm{Fe/H}] \lesssim -2.5$) model star at the beginning of the TPAGB phase in low- and intermediate-mass models. Panel (*b*) describes characteristics of the radiative ^{13}C-burning model. The process repeats in every thermal pulse cycle, and is made possible by the establishment, during the third dredge-up phase, of a small region centered on the dredge-up interface in which hydrogen and ^{12}C profiles overlap, and a subsequent conversion of the ^{12}C in this region into ^{13}C "pocket." In this model, *s*-process nucleosynthesis occurs during the interpulse phase in the ^{13}C pocket. See the text for further details.

Before the split into two parts of the initial, helium-driven convective shell occurs, some of the mixed-in hydrogen that has been captured by ^{12}C continues inward and, after the split, is trapped in the surviving helium convective zone as ^{13}N and/or as its daughter ^{13}C. At the high temperatures in the surviving helium convective shell, the reaction $^{13}\mathrm{C}(\alpha,n)^{16}\mathrm{O}$ occurs, with interesting consequences, as demonstrated by Iwamoto et al. (2004) for a 2 $M_{\odot}$ star with $[\mathrm{Fe/H}] = -2.7$.

To explore the ensuing neutron-capture nucleosynthesis in the helium convective shell, we adopt the same one-zone approximation used by Aikawa et al. (2001). Our nuclear network includes 59 isotopes of 16 light species from the neutron and ^{1}H through ^{31}P. Charged particle reaction rates are taken from Angulo et al. (1999) and Caughlan & Fowler (1988), and neutron-capture cross sections are taken from Bao et al. (2000). The model parameters of shell flashes are taken from the computation of the evolution of a 2.0 $M_{\odot}$ star (FII00) in which hydrogen is ingested by a helium convective zone. In this work, we treat the amount of mixed ^{1}H as a parameter since the

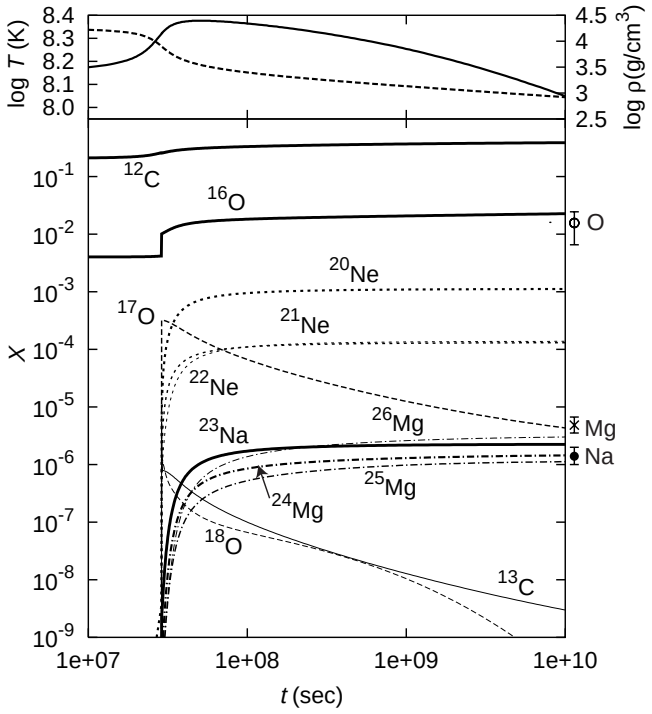

FIG. 4.—Lower panel shows the variation with time of isotopic abundances in a helium-flash–driven convective zone after ^{13}C has been mixed into the zone. The initial carbon isotope-abundance ratio in the zone is $^{13}C/^{12}C = 0.001$ and the abundance changes in the zone are driven by the release of neutrons in the $^{13}C(\alpha, n)^{16}O$ reaction. Instantaneous mixing of ^{13}C into the convective zone is assumed to take place at the peak stage of helium burning. The top panel shows the variations in the temperature (*solid line*) and in the density (*broken line*) during the helium flash for model parameters taken from the 2 $M_\odot$ star by Fujimoto et al. (2000). Element abundances (relative to carbon) observed for HE 0107−5240 are plotted at the right-hand side of the lower panel for O (*open circle*), Na (*filled circle*), and Mg (*cross*).

amount of ^{1}H mixed into the inner helium convective zone varies with the strength of the helium shell flash, and hence, with the stellar mass, and, also, depends on the treatment of convection. The mixing is assumed to occur at the peak of the shell flash.

Figure 4 illustrates the progress of nucleosynthesis in the helium convective zone in a Population III model star, unpolluted with accreted metals, when the amount of ^{13}C mixed into this zone is chosen in such a way that $^{13}C/^{12}C = 10^{-3}$ (M. Aikawa et al. 2004, in preparation). As soon as ^{13}C is mixed into the convective zone, it rapidly reacts with helium to produce neutrons. The neutrons so produced are captured primarily by ^{12}C to form ^{13}C and then reappear in consequence of additional $^{13}C(\alpha, n)^{16}O$ reactions. This neutron cycling process continues until the $^{16}O(n, \gamma)^{17}O$ reaction has converted most of the initially injected ^{13}C into ^{17}O. Then, α-capture on ^{17}O, which occurs $\sim 10^4$ times more slowly than capture on ^{13}C at the relevant temperatures, starts to produce neutrons via the reaction $^{17}O(\alpha, n)^{20}Ne$. The newly formed ^{20}Ne consumes neutrons to yield heavier isotopes of Ne and isotopes of Na and Mg.

The nature of *s*-process nucleosynthesis depends on whether or not seed nuclei are present in the helium convective zone. In second-generation stars, iron-group elements act as seeds for the production of heavy *s*-process isotopes by neutron capture. In first-generation stars, if no iron-group seed nuclei have entered the helium zone in consequence of the inward mixing of accreted iron-rich matter, most neutrons are absorbed by isotopes of Ne, Na, and Mg that are made by successive neutron captures and beta decays beginning with ^{20}Ne as a seed nucleus. The possible presence of iron-group seed nuclei due to pollution and mixing are discussed in § 4. The neutron-rich isotopes synthesized in a helium convective zone remain in place after convection ceases and some of them are incorporated into subsequent helium convective zones that appear during thermal pulses, as illustrated in Figure 3*a*. In case II′ models, after $[C/H] > -2.5$, neutron-rich isotopes made in the He-FDDM convective zone are dredged up to the surface along with carbon during third dredge-up episodes (FII00, and also see Iwamoto et al. 2004).

This mechanism for *s*-process nucleosynthesis works only for $[Fe/H] \lesssim -2.5$ (FII00), and contrasts with the mechanism of radiative ^{13}C burning that may operate in younger populations, as illustrated in Figure 2*b* (Straniero et al. 1995; see also Busso et al. 1999 and references therein).

The radiative ^{13}C-burning model invokes, by some extra-mixing mechanism that is assumed to operate during the third dredge-up phase, a partial mixing of hydrogen-rich matter with carbon-rich matter that was formed during the preceding helium shell flash in the convective zone driven by helium burning. In low-mass TPAGB stars, the temperatures across the interface between hydrogen-rich and carbon-rich zones become small enough during the dredge-up phase that carbon nuclei partially recombine with electrons, raising the opacity (Sackmann 1980); the opacity becomes proportional to the abundance of ^{12}C and semiconvection spreads out the ^{12}C and ^{1}H abundance profiles so that they overlap, producing in the hydrogen profile a long tail that descends inward with a gradual slope into the carbon-rich region (Iben, & Renzini 1982a, 1982b; Hollowell, & Iben 1989); finally, when hydrogen reignites in this region, proton capture on ^{12}C produces a ^{13}C "pocket." This mechanism works only for low-mass stars of low-metallicity (Iben 1983); in low-mass stars of higher metallicity, the contribution to the opacity by carbon ions is not large enough to activate semiconvection; in intermediate-mass TPAGB stars, the temperatures near the carbon-hydrogen interface do not become small enough for carbon to retain bound electrons. However, as discussed by Straniero et al (1995), the observations overwhelmingly suggest that α-capture on ^{13}C is the source of neutrons for *s*-process nucleosynthesis in low-mass Population I stars as well as in intermediate-mass stars of both the Population I and Population II variety, and that, therefore, some other mixing mechanism must also be operating. It is inferred that some form of convective overshoot and/or rotation-induced mixing must be capable of producing a region of overlapping ^{12}C and ^{1}H abundances, and that proton capture on ^{12}C subsequently produces a ^{13}C-rich pocket in all TPAGB stars (see e.g., Busso et al 1999).

Prior to the work of Straniero et al (1995), it was assumed that the ^{13}C in the ^{13}C pocket survives the interpulse phase and is incorporated intact into the next helium-flash–driven convective zone, with results similar to those found in the He-FDDM model (see e.g., Gallino et al. 1988; Hollowell, & Iben 1989; Hollowell et al. 1990; Busso et al. 1992). Straniero et al (1995) find instead that, because of compression brought about by the increase in core mass, temperatures in the ^{1}H-rich pocket rise sufficiently during the interpulse phase that ^{13}C captures α-particles and releases neutrons, driving *s*-process nucleosynthesis in the pocket, which remains in a radiative zone during the interpulse phase. The resultant *s*-process isotopes are mixed intact into the convective zone formed during the next helium shell flash, and no further *s*-process

nucleosynthesis occurs in the convective shell unless, as in the case of Population I and Population II stars, some ^{22}Ne is incorporated into the convective shell.

Using the ^{13}C-pocket scenario adopted by Goriely & Mowlavi (2000) for younger population stars, Goriely & Siess (2001) compute the radiative ^{13}C burning in a Population III star and argue that heavy elements such as Pb can be synthesized even if the stars initially lack iron-group elements. The differences between our results and theirs may stem from the following points:

1. We deal with neutron irradiation only once during the He-FDDM event, while they assume multiple irradiations during the occurrence of many (22) shell flashes, taken from a 3 $M_\odot$ model by Siess et al. (2002), which, differently from our model, undergoes carbon injection outward rather than hydrogen mixing inward.
2. In our convective ^{13}C-burning model, most neutrons are first converted into ^{17}O, and subsequent neutron-liberating reactions produce Ne isotopes with large neutron-capture cross sections at an abundance even larger than the abundance of ^{13}C added, while in the radiative ^{13}C-burning model, temperatures are too small for the reaction $^{17}\mathrm{O}(\alpha, n)^{20}\mathrm{Ne}$ to operate (Mathews et al. 1992). In our models, the Ne isotopes act as effective neutron absorbers, preventing the formation of heavy *s*-process elements.
3. The amount of ^{13}C injected into our convective zone is significantly smaller than the amount of ^{13}C postulated to be in the ^{13}C pocket of the radiative burning model. In our model, the separation of convective zones sets a limit and we assume a relatively small ratio of $^{13}\mathrm{C}/^{12}\mathrm{C} \simeq 10^{-3}$, whereas Goriely & Siess (2001) argue that the main contribution to heavy *s*-process elements comes from layers where $10^{-2} \lesssim {}^{13}\mathrm{C}/^{12}\mathrm{C} \lesssim 1$.

In any case, the outcome of radiative ^{13}C burning depends entirely on the abundance of ^{13}C in the postulated ^{13}C-rich pocket. Surely, the properties of the ^{13}C-rich pocket vary with the metallicity since, during a third dredge-up episode, metallicity differences affect the structure at the interface between the surface convective zone and the carbon-rich layer left behind by the helium-flash–driven convective shell. We return to this point in § 3.4, where we discuss comparisons with the observations.

3.3. *Oxygen and Sodium Enrichment*

The convective ^{13}C burning that occurs during the He-FDDM episode can be an effective mechanism for producing oxygen and sodium in stars of mass and metallicity in the case II′ category. In the absence of other competing neutron absorbers, the neutron recycling reactions $^{12}\mathrm{C}(n,\gamma)^{13}\mathrm{C}(\alpha, n)^{16}\mathrm{O}$ (Gallino et al. 1988) work effectively. When the Bao et al. (2000) neutron-capture cross sections are adopted, the final oxygen abundance produced through these reactions varies from 4.0×10^{-3} to 0.022 as the abundance ratio of mixed-in ^{13}C to ^{12}C is varied from $^{13}\mathrm{C}/^{12}\mathrm{C} = 10^{-4}$ to 10^{-2}. Correspondingly, the mass ratio of oxygen to carbon decreases from $^{12}\mathrm{C}/^{16}\mathrm{O} \simeq 10^2$ to $^{12}\mathrm{C}/^{16}\mathrm{O} \sim 10$. The final number of ^{16}O nuclei produced is much larger than the number of added ^{13}C nuclei with, on average, each added neutron being captured between ~200 and ~10 times by ^{12}C, depending on the amount of injected ^{13}C.

Another consequence of convective ^{13}C burning is the enrichment of neon, sodium and magnesium. As in the case of ^{16}O, the number of ^{20}Ne nuclei produced substantially exceeds the number of mixed-in ^{13}C nuclei, since some of the neutrons released via the $^{17}\mathrm{O}(\alpha, n)^{20}\mathrm{Ne}$ reaction are recaptured by ^{12}C and are recycled into ^{17}O and thence into ^{20}Ne. The final Ne abundance in the flash convective zone varies from 5×10^{-5} to $\sim 3 \times 10^{-3}$ as the initial ratio $^{13}\mathrm{C}/\,^{12}\mathrm{C}$ is varied from 10^{-4} to $\sim 10^{-2}$. Subsequent neutron captures on ^{20}Ne yield heavier isotopes of Ne, and, ultimately, to isotopes of Na and Mg. The sodium abundance increases from 10^{-7} to 10^{-5}, nearly in proportion to the abundance of the mixed-in ^{13}C.

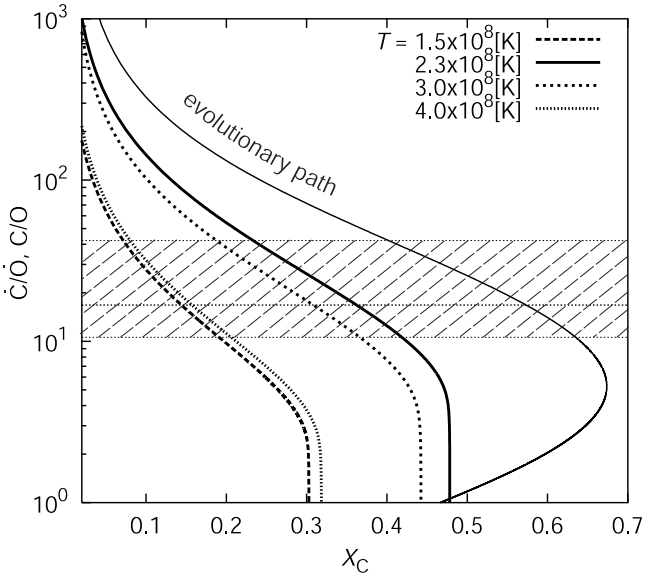

FIG. 5.—Ratio of the net production rate of carbon $\dot{C}$ to the production rate of oxygen $\dot{O}$ due to the 3α and $^{12}\mathrm{C}\alpha, \gamma^{16}\mathrm{O}$ reactions as functions of the carbon abundance by mass X_C, for the temperatures listed at the top right corner. The density has been set at 10^3 g cm^{-3}. For a given value of X_C, the helium abundance is set at $Y = 1 - X_C(1 + \dot{O}/\dot{C})$, and there exists a limiting value of X_C corresponding to $\dot{C} = 0$. The thick solid line gives the ratio for the temperature ($T = 2.3 \times 10^8$K) at which the ratio is a maximum at any given X_C. The thin solid line gives the evolutionary change in the C/O abundance ratio starting from pure helium (abundance by mass $Y = 1.0$) with $T = 2.3 \times 10^8$ K, for comparison's sake. The hatched area indicates the range in the C/O abundance ratio estimated from the spectroscopic data for HE 0107−5240.

If the total abundance of CNO isotopes in the envelope exceeds $[\mathrm{CNO/H}] \simeq -2.5$, the outer edge of the helium-flash convective zone cannot reach the base of the hydrogen-rich shell, and the He-FDDM mechanism no longer functions. Nevertheless, additional mechanisms operate to enrich oxygen and sodium during subsequent thermal pulses.

During a helium shell flash, ^{16}O is produced by α-capture on the ^{12}C made by the 3α reaction. Figure 5 shows, for four different temperatures, the ratio of the net production rate of ^{12}C to the production rate of ^{16}O by these reactions as a function of X_C, the abundance by mass of ^{12}C. Along the vertical axis, $\dot{O}$ is the rate of the $^{12}\mathrm{C}(\alpha, \gamma)^{16}\mathrm{O}$ reaction and $\dot{C}$ is the rate of the 3α reaction minus the rate of the $^{12}\mathrm{C}(\alpha, \gamma)^{16}\mathrm{O}$ reaction. For a given temperature, the ratio of production rates decreases rapidly with increasing X_C. For a given X_C, the $\dot{C}/\dot{O}$ ratio at first increases with increasing temperature and then decreases, with a sharp maximum occurring at $T \simeq 2.3 \times 10^8$ K. For values of $X_C \simeq 0.15 \sim 0.2$, typical in helium convective zones during recurrent helium shell flashes, if the temperature is not close to the maximum, the $\dot{C}/\dot{O}$ production-rate ratio can be smaller than several times 10, rapidly decreasing with increasing carbon abundance.

The thin solid curve in Figure 5 describes the evolutionary variation of the abundance ratio C/O at the fixed temperature $T = 2.3 \times 10^8$ K, starting with pure helium. For a given carbon abundance, the evolutionary abundance ratio is larger by a

factor of several (typically ∼3) than the production-rate ratio for the same carbon abundance. Accordingly, after an initial decrease achieved in a He-FDDM episode, it is possible, during the early stages of the third dredge-up phase in low-mass ($\leq 3\ M_\odot$) stars, to sustain relatively small C/O abundance ratios (as small as $C/O \lesssim$ a few tens) in the helium-flash convective zone where $X_C \simeq 0.15-0.2$. For more massive intermediate-mass stars, which begin TPAGB evolution with larger core masses, the maximum temperatures in the helium-flash convective zone are even higher ($T_{max} \gtrsim 4 \times 10^8$ K). In such stars, the abundance ratio C/O in the helium convective zone approaches the production rate $\dot{C}/\dot{O}$ for $X_C \simeq 0.2$ and abundance ratios as small as $C/O \simeq 10$ can be achieved even without benefiting from a precursor He-FDDM event.

With regard to Ne and Na isotopes, other enrichment channels also exist that do not hinge exclusively on the operation of a mechanism for mixing carbon-rich with hydrogen-rich material during third dredge-up episodes. In the helium flash convective zone, ^{22}Ne can be produced by the reactions $^{14}N(\alpha,\gamma)^{18}F(e^+\nu)^{18}O(\alpha,\gamma)^{22}Ne$. The ^{14}N can be produced in the hydrogen shell-flash–driven convective zone that appears during the He-FDDM event. If the stellar envelope is already CNO-enriched, ^{14}N is produced by quiescent hydrogen burning and is added to the helium core during the interpulse phase. If the core mass is small and the maximum temperature remains below $T_{max} = 4 \times 10^8$ K, ^{22}Ne survives the flash unburned and is added to the envelope by the following third dredge-up event, contributing to the surface enrichment of other neon isotopes formed during a possible precursor He-FDDM event.

Sodium can be formed during quiescent hydrogen burning as some neon isotopes are converted into Na through the Ne-Na cycle reactions. At the temperatures prevalent in the hydrogen-burning shell during the early TPAGB phase in the stars of concern here, the Na abundance produced by Ne-Na chain reactions is rather small (about a few percent of Ne), and yet, thanks to the large enrichment of Ne isotopes, this can amount to a significant overabundance of Na relative to the scaled-solar abundance. When formed, Na can survive the helium flash, be dredged up by surface convection and contribute to a surface enrichment. It is to be noted that ^{24}Mg is also produced through the Ne-Na chain reactions in the quiescent hydrogen-burning shell, although the amount produced depends strongly on the branching ratio between the (p, α) and (p, γ) reactions on ^{23}Na (Angulo et al. 1999; see also Aikawa et al. 2001).

As a corollary, O and Na enrichments coupled with C and N enhancements are a symptom of TPAGB evolution in which both the He-FDDM mechanism and the third dredge-up mechanism have worked.

3.4. *Comparisons with the Observations*

Recent observations reveal the peculiar aspects of the most metal-poor stars. One of the major characteristics of these stars is a large frequency of carbon stars. This frequency is ∼25% for known stars with $[Fe/H] < -3$, a frequency far larger than the few percent for Population I and Population II stars (Rossi et al. 1998). The Hamburg/ESO objective-prism survey confirms that, among EMP stars, there is a high frequency of stars with strong carbon-enhancements (N. Christlieb 2004, private communication).

As pointed out by FII00, the large frequency of carbon stars among EMP stars can be explained by the occurrence of the He-FDDM mechanism, which enables such stars to become carbon stars for a wider mass range and at an earlier phase of evolution than can stars of younger populations. The initial stellar masses of stars that can become carbon stars in this way span the entire mass range below ∼3 $M_\odot$ of stars that can evolve off the main sequence in a Hubble time, including the low masses for which the third dredge-up cannot work in younger populations. Thus, the fraction of EMP stars that can end their nuclear-burning careers as carbon stars is much larger than the fraction of Population I and Population II stars that can do so. In addition, because of a smaller core mass and smaller CNO abundances, when an EMP star evolves into a carbon star, its radius is much smaller than that of a carbon star belonging to younger populations; this means that EMP binary systems that produce carbon stars can have smaller initial orbital separations than can younger generation binary systems that produce carbon stars. Most currently observed carbon stars owe their spectral peculiarity to prior mass transfer from an initially more massive component in a binary system; this fact, coupled with the larger fraction of EMP binary systems that can accommodate TPAGB stars and the larger range of masses for progenitors of EMP carbon-rich stars (compared with their counterparts among younger generations) may account for the large fraction of carbon stars among EMP stars. Moreover, many EMP carbon stars exhibit large enhancements of N and very large enhancements of C, with $[C + N/Fe] \gtrsim 2$ and $[C + N/H] = 0 \sim -1$, consistent with theoretical predictions.

Among EMP carbon stars, there is a correlation between the abundances of carbon and nitrogen and the abundances of *s*-process elements, as pointed out by Aoki et al. (2002a). In a diagram similar to theirs, we show in Figure 6 the Ba or Pb enhancement versus the C(+N) enhancement for stars with metallicities in the range $-3.75 \leq [Fe/H] < -2.5$. Data has been taken from Ryan et al. (1991), Norris et al. (1997a, 1997b, 2001), Hill et al. (2000, 2002), Aoki et al. (2001, 2002a, 2002b), Depagne et al. (2002), Johnson & Bolte (2002), Cohen et al. (2003), Lucatello et al. (2003), and Sneden et al. (2003). Filled circles, open circles, and crosses denote, respectively, the coordinates [Ba/Fe] versus $[C + N/Fe]$, [Pb/Fe] versus $[C + N/Fe]$, and [Ba/Fe] versus [C/Fe]. In the figure, stars are clearly separated into two branches, one with and one without *s*-process element enhancements. The C(+N) enhancement covers the same range on both branches, namely, $[C(+N)/Fe] \simeq 0 \sim 2.5$. On the *s*-process–enriched branch, the abundance of *s*-process elements increases, with increasing C(+N) abundance, over a range of ∼100 or more. For stars in the chosen metallicity range, there are two different evolutionary paths to the carbon stars, case II and case II′, which are separated by the nature of enhancements during third dredge-up episodes following the occurrence of a He-FDDM event. These two paths may correspond to the two branches evident in Figure 6, case II to the branch without *s*-process element enrichment and case II′ to that with *s*-process element enrichment. The theoretically predicted abundance characteristics for each case, indicated by the large open circles in Figure 6, actually coincide with the abundance characteristics at the rightmost end of each branch. In case II models, the C and N enrichments are produced only by the He-FDDM mechanism, with a relatively large nitrogen enrichment and without a significant enhancement of *s*-process elements. In case II′ models, third dredge-up episodes, following a He-FDDM episode, give rise to the enhancement of *s*-process elements as well as to a decrease in the N/C ratio because of the production of ^{12}C by the 3α reaction. This is in agreement

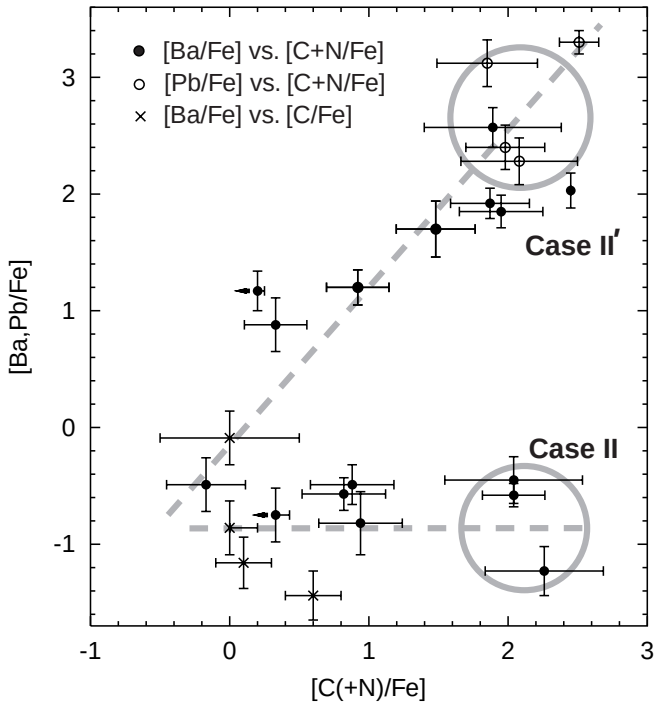

FIG. 6.—Distribution of EMP stars ([Fe/H] < -2.5) with regard to the enhancement of *s*-process elements versus the enhancement of carbon and nitrogen. Literature sources are given in the text. The existence of two distinct branches defined by the observed abundances is emphasized by a dashed line through each branch. The large open circles at the right-hand ends of the two branches indicate the abundances of CN and *s*-process elements predicted, respectively, by case II and case II′ evolutionary models. Along each branch, the observed abundances are interpreted to be the result of mixing, in a binary star system, between the pristine envelope matter of a low-mass component and enriched matter transferred from a more massive TPAGB star component.

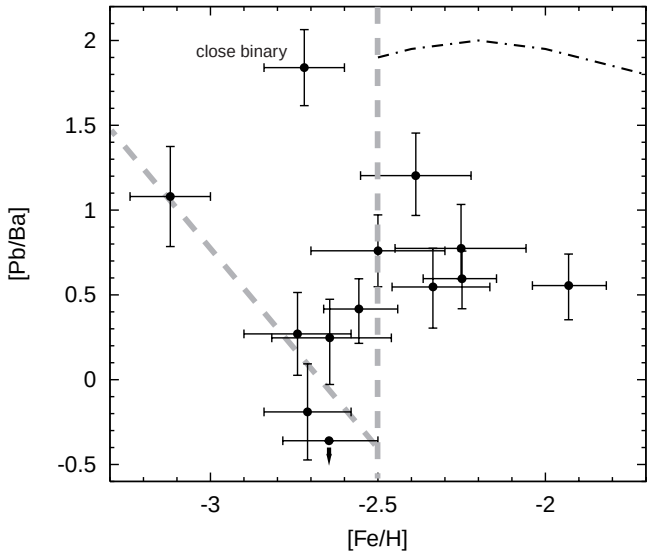

FIG. 7.—Variations of the Pb/Ba ratio vs. the metallicity. Literature sources are given in the text. A break in the observed distribution is discernible near [Fe/H] $\simeq -2.5$, with ratios of 0.5–1.2 on the larger metallicity side, and ratios of -0.5–0.5 on the smaller metallicity side. This break may be interpreted as being due to a switch in the mechanism of *s*-process nucleosynthesis from radiative ^{13}C burning for Population I and Population II stars to convective ^{13}C burning for EMP stars. The star HE 0024−2523, with [Fe/H] $= -2.7$, is in a short period binary ($P_{\rm orb} = 3$ days), and the large [Pb/Ba] ~ 1.84 for this star may be attributed to the effects on interior *s*-process nucleosynthesis of the common envelope evolution that the binary star experienced while the primary was in the TPAGB phase (Lucatello et al. 2003). Excluding the point for the close binary star, one could argue that, for [Fe/H] < -2.5, the Pb/Ba ratio increases with decreasing metallicity. Such a trend is consistent with the predictions of the He-FDDM convective ^{13}C-burning model. The dash-dotted line in the region [Fe/H] > -2.5 is the ratio predicted by an *s*-process nucleosynthesis model (Busso et al. 1999) based on the radiative ^{13}C-burning model (Gallino et al. 1998).

with the fact, pointed out by Ryan et al. (2003), that the degree of processing by CN-cycle reactions is clearly greater in stars without *s*-process element enhancements than in stars with *s*-process element enhancements.

It has also been pointed out (Aoki et al. 2000, 2001, 2002b; Ryan et al. 2001) that metal-poor stars exhibit interesting variations in the relative abundances of *s*-process elements of different atomic weight. We have reviewed in § 3.2 two distinct sites for *s*-process nucleosynthesis when the ^{13}C$(\alpha, n)^{16}$C reaction is the neutron source: (1) a convective helium- and carbon-rich shell (convective ^{13}C burning) during a helium-shell flash and (2) a helium- and carbon-rich radiative zone (radiative ^{13}C burning) during the interflash phase. The convective site arises naturally in EMP model stars within the framework of the current standard theory of stellar evolution. On the other hand, *s*-process nucleosynthesis in a radiative site requires the formation of an appropriate ^{13}C pocket by either semiconvective mixing (which has been shown to occur in low-mass models of Population II metallicity) or by convective overshoot and/or by rotation induced mixing across a carbon-hydrogen interface during the third dredge-up phase. From an analysis of the distribution of *s*-process elements in the younger populations (see the review by Busso et al. 1999), it has been concluded that the overshoot must occur. The radiative ^{13}C-burning model (with the ^{13}C made possible by convective overshoot) predicts that the heavier *s*-process elements are produced at higher abundances in stars of lower metallicity since the number of neutrons available per seed nucleus increases with decreasing metallicity unless the amount of ^{13}C of the ^{13}C pocket decreases proportionately.

In Figure 7 the ratio of Pb to Ba, relative to solar, is plotted against the stellar metallicity. Data are taken from Aoki et al. (2001, 2002b), Johnson & Bolte (2002), Cohen et al. (2003), and Lucatello et al. (2003). The figure shows clearly that Population II stars with [Fe/H] > -2.5 exhibit a large Pb/Ba ratio, of the order of 10 times larger than the solar value, at least qualitatively in agreement with the prediction of the radiative ^{13}C-burning model. In addition, Van Eck et al. (2001, 2003) find, for CH stars with [Fe/H] > -2.45, enhancements by a factor of $\sim$10 in the ratio of Pb to the main *s*-process elements.

However, a sharp difference in the Pb/Ba ratio is discernible at the metallicity [Fe/H] $\simeq -2.5$. Just below this metallicity, with one exception, Pb/Ba ratios are smaller, by up to a factor of 10 or so, than those above this metallicity. The exception is HE 0024−2523, with [Fe/H] $\simeq -2.7$ and [Pb/Ba] $\simeq 1.8$ (Lucatello et al. 2003). This star is known to be in a binary system of short period ($\sim$3 days) and small semimajor axis ($\sim 10\ R_\odot$). It is likely, as suggested by Lucatello et al. (2003), that the precursor of the present binary experienced a common envelope event when the original primary became a TPAGB star and that the common envelope evolution affected the nucleosynthesis in the primary, leading to a distribution of *s*-process elements different from that occurring in an isolated TPAGB star.

The sudden decrease in the Pb/Ba ratios at [Fe/H] $\simeq -2.5$ for stars that are not in a close binary suggests that radiative ^{13}C burning in a ^{13}C-rich pocket during a third dredge-up episode is either dominated by or replaced by convective ^{13}C burning.

In the convective ^{13}C-burning model, ^{13}C is mixed into a helium convective zone that is much more massive than the expected mass in the ^{13}C pocket (e.g., see Busso et al. 1999). The mass of the mixed-in ^{13}C cannot be much larger than assumed in the ^{13}C pocket (Gallino et al. 1988; Goriely & Mowlavi 2000) since the splitting of the convective zone places a ceiling on the amount of ^{13}C produced and carried down into the lower helium convective zone before the splitting occurs. Accordingly, in the convective ^{13}C-burning model, the number of available neutrons per seed nucleus can be smaller compared with the number available in the radiative ^{13}C-burning model, which may lead to a sudden decrease in the [Pb/Ba] ratio if there is a switchover in the mechanism of *s*-process nucleosynthesis.

Alternatively, Aoki et al. (2002b) argue that, for metallicities $[Fe/H] \simeq -2.5$, the observations suggest a trend in the [Pb/Ba] versus [Fe/H] diagram, with [Pb/Ba] decreasing with decreasing [Fe/H]. However, the suggested trend is spoiled by the existence of the star CS 22183−015, which, at a metallicity $[Fe/H] \simeq -3.1$, has [Pb/Ba] much larger (Johnson & Bolte 2002) than that of most stars of metallicity $[Fe/H] \sim -2.5 \pm 0.3$. The neutrons per seed made available in the *s*-process nucleosynthesis event responsible for the abundances in CS 22183−015 were larger by a factor of 3–4 than those made available in the events responsible for these abundances in stars with metallicities in the range $-2.8 < [Fe/H] < -2.5$. Also in the convective ^{13}C-burning model, the number of available neutrons per seed nucleus increases in inverse proportion to the abundance of iron-group elements, and this is, at least qualitatively, in accord with the difference in the [Pb/Ba] ratio between CS 22183−015 and the stars with metallicities in the range $-2.8 < [Fe/H] < -2.5$. In the binary scenario with convective ^{13}C burning, dispersions in the ratios of *s*-process elements among individual secondaries of similar metallicities may be ascribed to variations in the amount of ^{13}C mixed into the convective zone; this amount might be expected to vary with the initial mass of the primary. In this interpretation, a perceived trend in the element ratios for stars with metallicities in the range $-2.8 < [Fe/H] < -2.5$ is instead dispersion about a mean.

Finally, we note that there is no observational evidence pointing to the operation of the radiative ^{13}C-burning mechanism below $[Fe/H] \simeq -2.5$. Currently available observations are limited, and, certainly, more observational data on the Pb/Ba ratio, especially for the lowest metallicities, are needed to help clarify the situation and to allow definitive conclusions to be drawn.

Although the efficiency of the convective-overshoot mechanism that prepares conditions for the formation of a ^{13}C pocket has yet to be established as a function of environmental conditions, it is natural to suppose that, since the metallicity surely affects the thermal structure near the boundary between the surface convective zone and the carbon-rich helium core during the third dredge-up episode, this efficiency may change with the metallicity. It is worth noting that, even for stars with $[Fe/H] > -2.5$, the observed Pb/Ba ratios are small compared with those expected from *s*-process nucleosynthesis models that rely on a neutron source that does not depend on the metallicity. In Figure 7 we plot the Pb/Ba ratios predicted by Busso et al. (1999) for a particular choice of ^{13}C-pocket characteristics (Gallino et al. 1998). The predicted values all lie above the observed values by more than a factor of $\sim$10. This may again indicate that the strength of the neutron source in Population I stars is larger than the strength of the neutron source in Population II stars. One possibility is that the primary mechanism that sets the stage for the formation of the ^{13}C pocket switches from overshoot mixing to semiconvective mixing as the metallicity drops below a critical value. The semiconvective mixing mechanism has been demonstrated to work for the metallicity $Z = 0.001$ (Hollowell, & Iben 1989) and, because of the character of the mixing, the ratio of protons to ^{12}C in the mixed region can be smaller than expected in the case of overshoot mixing, leading ultimately to a smaller abundance of ^{13}C in the ^{13}C-pocket. Further investigation is necessary to determine how the conditions for the formation of a ^{13}C-pocket vary with the metallicity. For EMP stars that have experienced the He-FDDM event, the opacities in radiative regions are dominated by the carbon dredged-up into the envelope at the end of this event, so semiconvection is not expected to play a role in producing a ^{13}C pocket in them.

4. THE ORIGIN OF HE 0107−5240

In this section we examine again the scenarios presented in § 2 for the origin of HE 0107−5240, this time taking advantage of the theoretical and observational knowledge reviewed in § 3. We focus first on scenarios that assume that the observed carbon enrichment was acquired after birth. HE 0107−5240 exhibits large excesses of carbon and nitrogen and $C/N = 40 \sim 150$ (Christlieb et al. 2002, 2004). Since single low-mass Population III stellar models develop an abundance ratio $C/N \simeq 1$ as red giants (case I; $\leq 1.1\ M_\odot$ Hollowell et al. 1990; Fujimoto et al. 2000; Schlattl et al. 2002), the possibility of an evolved, single Population III star is excluded. Since HE 0107−5240 is a red giant of metallicity less than $[Fe/H] \simeq -4.5$, the case II model cannot be applied.

However, the Population III binary scenario, with a primary component of the case II′ variety, is a viable possibility. Since model stars of metallicity $[Fe/H] \lesssim -4.5$ share common evolutionary characteristics, the second-generation binary scenario, with metallicity at birth being the same as presently observed, is also a possibility. Accordingly, we postulate in the following that HE 0107−5240 is either a first- or second-generation star, formed out of matter in a primordial cloud, and formed in a binary system in which it was the secondary of mass $M_s \simeq 0.8\ M_\odot$ and in which the primary was of initial mass in the range $1.2 \leq M_p/M_\odot \leq 3.0$. The primary component has followed case II′ evolution and achieved enrichment of C, N, O, and Na by experiencing a He-FDDM event and subsequent third dredge-up events, as discussed in § 3.

Figure 4 shows the element abundances resulting from neutron-capture nucleosynthesis in the helium-flash convective zone during a He-FDDM event for a model in which the abundance of ^{13}C mixed into the helium-flash–driven convective zone, relative to the abundance of ^{12}C in the zone, is $^{13}C/^{12}C = 0.001$. The abundances of ^{16}O and of Mg and Na isotopes have reached their final values at the right-hand side of the figure. Along the right-hand ordinate in the figure are placed the abundances relative to carbon of O (*open circles*), Mg (*crosses*), and Na (*filled circles*) observed for HE 0107−5240. For O, Na, and Mg, the observed ratios can be well reproduced by the calculated abundance ratios to carbon in the helium convective zone. As discussed in § 3.3, the abundances of C and O as well as Na, achieved during a He-FDDM episode are not expected to be changed much in the helium-flash convective zones that appear during the following TPAGB phase. In Figure 5 the shaded region gives the range in the C/O abundance ratio estimated from the observations of HE 0107−5240. An abundance ratio in the observed range is achieved

during helium shell flashes in model stars of mass $M \leq 3\,M_{\odot}$ if temperatures near $T \simeq 2.3 \times 10^8$ K are not reached.

The surface enrichment of carbon in the primary component depends upon what fraction of the matter once contained in the helium-flash–driven convective zone during the He-FDDM episode and the following third dredge-up episode is carried outward into the convective envelope. Denoting the mass of dredged-up material by $\Delta M_{\rm du}$, we have the surface carbon abundance, $X_{12,\,p,\,\rm env}$, in the envelope of the primary by mass at

$$X_{12,\,p,\,\rm env} = X_{12,\,\odot}\left(\frac{\Delta M_{\rm du}}{0.03\ M_{\odot}}\right)\left(\frac{1.5\ M_{\odot}}{M_{p,\,\rm env}}\right)\left(\frac{X_{12,\,p,\,\rm He}}{0.15}\right), \quad (8)$$

where $M_{p,\,\rm env}$ is the mass in the envelope of the primary, $X_{12,\,p,\,\rm He}$ is the carbon abundance by mass in the helium convective zone of the primary, and $X_{12,\,\odot}$ is the solar carbon abundance by mass (=3.0×10^{-3}; Anders & Grevesse 1989). The mass in the helium-flash–driven convective zone falls in the range ≃a few times 10^{-2} to several times $10^{-3}\ M_{\odot}$, and equation (8) indicates that only a small fraction of this, or $\Delta M_{\rm du} \sim 3.5 \times 10^{-5} M_{p,\,\rm env} X^{-1}_{12,\,p,\,\rm He}$ is enough to enrich the envelope above $[{\rm CNO/H}] = -2.5$. As a corollary, we note that this is sufficient to prevent another He-FDDM event from occurring.

Immediately after the He-FDDM episode, the C/N ratio in the envelope of the primary is ∼5. Subsequently, the C/N ratio increases as ^{12}C is added to the envelope during successive third dredge-up events. In order for the C/N ratio to reach the observed range, 8–30 times as much carbon has to be added by third dredge-up episodes as is added by the He-FDDM episode. If approximately a few times $10^{-3}\ M_{\odot}$ is added by the He-FDDM episode, third dredge-up episodes will cause the C/H ratio at the surface of the primary to approach, or even exceed, the solar C/H ratio. The ^{12}C/ ^{13}C ratio at the surface of the primary at the beginning of the mass-transfer event can be estimated if we assume that, during the He-FDDM episode, the ^{12}C/ ^{13}C ratio in the hydrogen-flash convective region attains the equilibrium value of ∼4. Dredge-up following the He-FDDM event leads to a similar carbon isotopic abundance ratio at the surface. Then, 8–30 subsequent third dredge-up episodes (during which only the isotope ^{12}C is added) lead to a surface ratio $^{12}{\rm C}/^{13}{\rm C} \sim 32$–120, which is consistent with the estimate for HE 0107−5240 of $^{12}{\rm C}/^{13}{\rm C} > 50$ (Christlieb et al. 2004).

As the enhancement of carbon in its envelope progresses, the primary brightens and expands in response to the increase in the abundance of CNO catalysts and the corresponding increase in the burning rate of its hydrogen-burning shell. Finally, the primary loses its hydrogen-rich envelope either through Roche lobe overflow or through wind mass loss; in either case, some envelope matter falls onto the secondary. The amount of mass that must be transferred from the primary to the secondary to produce the surface carbon abundance $[{\rm C/H}] = -1.3$ observed for HE 0107−5240 may be estimated as

$$\Delta M_{\rm acc} = 0.01\ M_{\odot}\left(\frac{X_{12,\,\odot}}{X_{12,\,p,\,\rm env}}\right)\left(\frac{M_{s,\,c\ \rm env}}{0.2\ M_{\odot}}\right), \quad (9)$$

where $M_{s,\,c\ \rm env}$ is the mass of the envelope convective zone of the secondary after mass transfer ceases. The fact that $\Delta M_{\rm acc}$ is only a small fraction of the initial envelope mass of the primary suggests that mass transfer occurs via accretion from a wind rather than through Roche lobe overflow, in agreement with the analysis given by Iben (2000). In the case of accretion from a wind, the mass-accretion rate onto the secondary may be estimated from the gravitational focusing cross section defined by equations (1) and (2). For a spherically symmetric wind, the mass $\Delta M_{\rm acc}$ accreted by the secondary is simply the mass $\Delta M_{\rm loss}$ lost by the primary times the solid angle formed by the gravitational focusing cross section at a distance equal to the separation a of the binary components. Thus,

$$\Delta\, M_{\rm acc} = \frac{\sigma_{\rm acc}}{4\pi a^2}\,\Delta M_{\rm loss}. \quad (10)$$

From this relationship, we may estimate the semimajor axis of the binary system at the start of mass transfer as

$$a \simeq 18\ {\rm AU}\left(\frac{M_s}{0.8\ M_{\odot}}\right)\left(\frac{0.01\Delta M_{\rm loss}}{\Delta M_{\rm acc}}\right)^{1/2}\left(\frac{20\ {\rm km\ s^{-1}}}{v_{\rm rel}}\right)^2, \quad (11)$$

where $v_{\rm rel}$ is velocity of the wind relative to the velocity of the secondary (the vector difference of orbital velocity and wind velocity). If the wind carries away matter with the same specific angular momentum as resides in the orbital motion of the primary, the orbital separation increases by a factor inversely proportional to the total mass of the system (Jean's theorem). Accordingly, the resultant orbital period $P_{\rm orb}$ of the system at the end of mass transfer could be of the order of

$$P_{\rm orb} \simeq 76\ {\rm yr}\left(\frac{M^{3/2}_{\rm total,0}}{M^2_{\rm total}}\right)\left(\frac{M_s}{0.8\ M_{\odot}}\right)^{3/2}\left(\frac{0.01\Delta M_{\rm loss}}{\Delta M_{\rm acc}}\right)^{3/4} \times \left(\frac{20\ {\rm km\ s^{-1}}}{v_{\rm rel}}\right)^3, \quad (12)$$

where $M_{\rm total,\,0}$ and $M_{\rm total}$ are, respectively, the total mass of the binary before and after the completion of mass transfer.

Since the wind escapes the primary with a speed of the order of the sound speed at the surface of the primary (∼10 km s^{-1}) and the orbital speed of the secondary is of comparable magnitude, we may estimate $v_{\rm rel} \sim 20$ km s^{-1}. Thus, after mass transfer is completed, the separation and period of the binary could be increased up to $a \simeq 34$ AU and $P_{\rm orb} \simeq 150$ yr with $M_{\rm total} \simeq 1.5\ M_{\odot}$ and $M_{\rm total,\,0} \simeq 2.8 M_{\odot}$. Such a long period is not excluded by the observations, which, to date, cover only 52 days in one case (Christlieb et al. 2004) and 373 days in another (Bessell et al. 2004). The above estimate predicts a variation in the velocity, v_r, in the radial direction at an order of $dv_r/dt \simeq 0.11 \sin i \sin\theta$ km s^{-1} yr^{-1}, where i and θ are the inclination angle and the orbital position angle, respectively. This remains well below the 1 σ scatter of the radial velocity measurement of HE 0107−5240, which is currently 44.5 ± 0.5 km s^{-1} (Christlieb et al. 2004).

The argument concerning abundances that we have presented applies to a binary system of either the first or second generation, independent of whether the iron-group elements are acquired after birth or are present at birth. With regard to *s*-process elements, however, it does make a difference whether or not seed nuclei exist in the helium-flash convective zone. If HE 0107−5240 is a second-generation star, the *s*-process elements are synthesized with iron-group elements as seed nuclei in the lower helium convective shell during the

He-FDDM episode. Since the iron abundance of HE 0107−5240 is smaller by a factor of more than ∼100 than the iron abundances of most other known EMP stars, the number of neutrons available per seed nucleus ought to be larger in HE 0107−5240 by the same factor. Even if convective ^{13}C burning is responsible for the synthesis of heavy *s*-process elements, very large Pb/Ba ratios would be expected. As most of the iron-group elements are converted into heavy *s*-process elements, the overabundance of lead in the helium-flash convective zone is given by the number ratio of Fe to Pb in the solar distribution, namely, $(Y_{\rm Fe}/Y_{\rm Pb})_\odot = 3\times10^5$. In the binary scenario, the *s*-process elements produced in the He-FDDM event are first diluted by mixing into the convective envelope of the AGB primary and then, after transfer via a wind to the secondary, by mixing into the convective envelope of the secondary when it becomes a red giant. Hence, the overabundance at the surface of HE 0107−5240 becomes

$$[{\rm Pb/Fe}] \simeq \log\left[\left(\frac{Y_{\rm Fe}}{Y_{\rm Pb}}\right)_\odot \left(\frac{f\Delta M_{\rm du}}{M_{p,\,\rm env}}\right)\left(\frac{\Delta M_{\rm acc}}{M_{s,\,c,\,\rm env}}\right)\right] \quad (13)$$

$$\simeq 2.5 + \log\left[\, f\,\left(\frac{0.15}{X_{12,\,p,\,\rm He}}\right)\right], \quad (14)$$

where $\Delta M_{\rm du}$ is the mass of dredged-up material and f is the fraction of this dredged-up material that has been exposed to neutron irradiation during the He-FDDM event. Since a significant fraction r of matter is incorporated into helium-flash convective zones during subsequent thermal pulses, $f = \sum_n^{8\sim30} r^n/(8\sim30) \simeq 0.2 \sim 0.05$ for $r \simeq 0.6$ (Iben 1977). Consequently, an overabundance of lead ([Pb/Fe] $\simeq 1 \sim 2$) ought to be observed for HE 0107−5240 if it really is a second-generation star.

On the other hand, if HE 0107−5240 is a first-generation star, two different pictures are possible, depending on whether or not accreted metals can be carried into the helium convective zone during the He-FDDM episode. The primary component may accrete metal-polluted gas in the primordial gas cloud and carry these metals inward as surface convection deepens at the time of the second dredge-up phase. In Figure 8 the dotted line shows the deepest reach of surface convection during the second dredge-up phase as a function of the mass of a Population III model star in the mass range $1.2 \le M/M_\odot \le 3.0$. In real counterparts of the model stars, metals accreted onto surface layers are spread uniformly throughout the shaded area shown in the figure. Solid lines show the location of the base and outer edge of the convective shell formed in the He-FDDM event at the moment that the outer edge touches the base of the hydrogen profile.

There is a critical mass, $M_{\rm crit} \simeq 2.5\ M_\odot$, such that, for an initial mass $M_{\rm initial} < M_{\rm crit}$, the He-FDDM convective shell remains below the polluted (*shaded*) area and heavy *s*-process elements built-up from iron-group seed nuclei will not be produced. In contrast, for an initial mass $M_{\rm initial} > M_{\rm crit}$, the He-FDDM convective shell extends into or lies completely in the polluted (*shaded*) area and heavy *s*-process elements are built-up from iron-group seed nuclei. Penetration into the polluted area has been made possible by the fact that, following a second dredge-up episode and prior to the He-FDDM episode, hydrogen burning during the EAGB phase of evolution has moved the hydrogen-helium interface into the metal-polluted zone. In this case, however, the degree of enhancement varies with the degree of metal contamination that the primary has experienced during its relatively short lifetime in the polluted primordial cloud. On average, a less massive star (lifetime $t \sim 4.1\times10^8$ yr for $M_{\rm initial} = 2.5\ M_\odot$) will experience more contamination than a more massive star (lifetime $t \sim 2.6\times10^8$ yr for $M_{\rm initial} = 3.0\ M_\odot$)

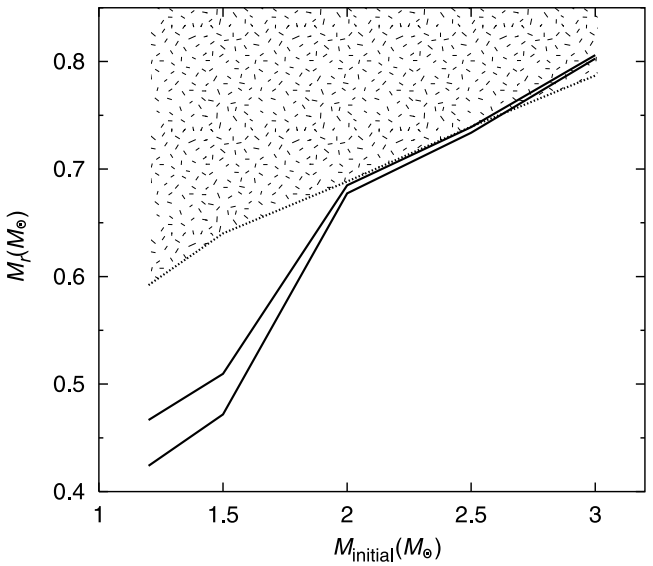

FIG. 8.—Deepest reach of surface convection during the second dredge-up phase (*dotted line*) and the locations of the top and bottom of the He-FDDM convective zone when the top extends through the base of the hydrogen profile (*solid lines*), plotted as functions of the initial mass of Population III model stars. The hatched area identifies the zone into which surface convection can carry accreted metals. There exists a critical mass, $M_{\rm crit} \simeq 2.5\ M_\odot$, such that, for $M_{\rm initial} < M_{\rm crit}$, the He-FDDM convective zone is confined to the metal-free zone, while for $M_{\rm initial} > M_{\rm crit}$, it extends into or lies entirely in the metal-polluted zone. This penetration has been made possible by the fact that, prior to the He-FDDM episode, model stars of mass $M_{\rm initial} > M_{\rm crit}$ have experienced a second dredge-up episode and hydrogen shell burning during the following EAGB phase of evolution has moved the hydrogen-helium interface into the metal-polluted zone.

Our results for the binary scenario are summarized in Figure 9. Our proposal is that HE 0107−5240 has evolved from a secondary component (of mass ∼0.8 $M_\odot$) in a wide binary system with a primary (of initial mass between 1.2 and 3 $M_\odot$) that has undergone case II′ evolution and thereafter transferred via a wind a small amount of mass to the secondary. The lower boundary of the mass range in Figure 9 is determined by the condition that the third dredge-up takes place after the surface CNO abundance grows larger than $[{\rm CNO/H}] \gtrsim -2.5$. Our binary scenario gives a reasonable account of the observed abundances of C, N, O, and Na, and of the carbon isotopic ratio $^{12}C/\,^{13}C$, independently of whether the binary system is composed of first-generation stars that accrete metals after birth or of second-generation stars, formed of gas that has already been contaminated with metals.

Clues to the origin of an observed metallicity can be obtained by observing the relative abundances of heavy *s*-process elements. If, for example, [Pb/Ba] ∼ 0, HE 0107−5240 may be identified as a Population III star born in a binary system with a primary component of mass $M_{\rm initial} < M_{\rm crit} (\simeq 2.5\ M_\odot)$. If, on the other hand, [Pb/Fe] = 1 ∼ 2, HE 0107−5240 may be identified as possibly being a second-generation star. A Pb overabundance is also consistent with the primary being a Population III star with $M_{\rm crit} < M_{\rm initial} \lesssim 3\ M_\odot$, but the degree of enhancement depends upon the efficiency of metal accretion in the primordial cloud. Presently, we have only upper limits on the abundances of heavy *s*-process elements: [Sr/Fe] < −0.52,

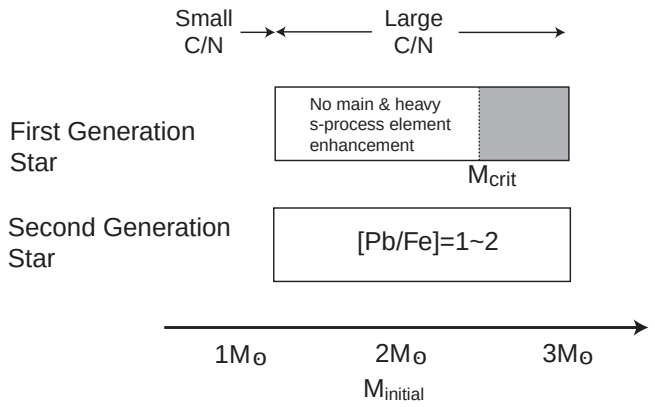

FIG. 9.—Illustration of the proposed binary scenario showing the mass range of the primary component allowed by the currently observed abundances of C, N, O, and Na in the spectrum of HE 0107−5240. The upper box is for a first-generation binary, having acquired metals through accretion after birth, and the lower box is for a second-generation binary. The allowed mass range corresponds to case II′ defined by FII00. Predictions regarding *s*-process nucleosynthesis are given in the boxes. For a first-generation binary, no enhancement in *s*-process elements occurs if the initial primary mass is smaller than $M_{\rm crit} \simeq 2.5$; an enhancement occurs if the primary has an initial mass greater than $M_{\rm crit}$ (but less than 3 $M_\odot$) and has accreted metals before experiencing the He-FDDM event. For a second-generation binary, an overabundance of heavy *s*-process elements as large as $[{\rm Pb/Fe}] = 1 \sim 2$ is expected. A primary of mass less than that indicated in the figure cannot produce a sufficiently large C/N ratio to account for the observations, while the helium—flash–driven convective zone in a primary more massive than indicated cannot reach the hydrogen-rich envelope.

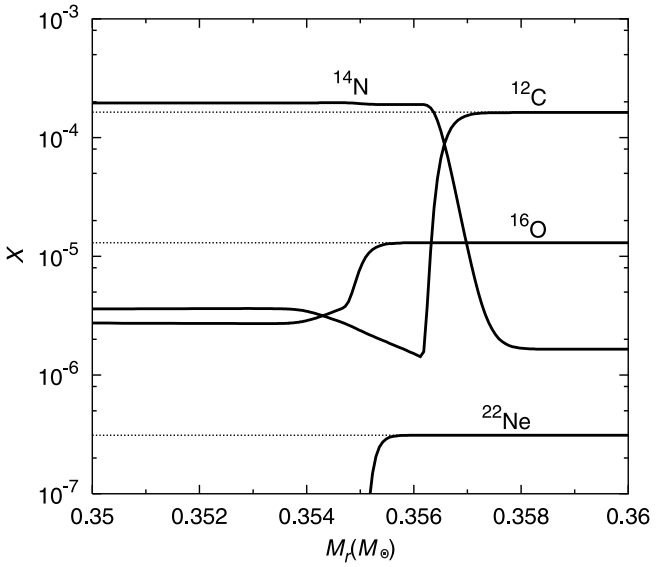

FIG. 10.—Abundance modifications due to the first dredge-up are shown for a 0.8 $M_\odot$ model star with the same C and O abundances as HE 0107−5240. The surface abundance of nitrogen increases to $[{\rm N/H}] = -2.8$, which falls within the observed range of $[{\rm N/H}] = -2.7 \sim -3.0$. In order to see the change in the sodium abundance, we add ^{22}Ne, but it cannot burn in the upper part of the hydrogen-burning shell that is eventually mixed into the envelope during the first dredge-up episode, so no enrichment of sodium is obtained.

$[{\rm Ba/Fe}] < 0.82$, $[{\rm Eu/Fe}] < 2.78$ (Christlieb et al. 2002, 2004). These limits are consistent with our models, but not definitive confirmation. In order to establish the origin of HE 0107−5240 unambiguously, we need abundances rather than limits for these ratios and, most importantly, we require the ratio Pb/Ba.

Finally, we follow the evolution to the RGB of a 0.8 $M_\odot$ model star with the C and O abundances observed for HE 0107−5240 and investigate the modifications of the surface abundances along the RGB. We add ^{22}Ne to see the effect on the ^{23}Na abundance. Figure 10 shows the abundance distribution in the envelope initially (*dotted lines*) and sometime after the first dredge-up event has taken place (*solid lines*). At its maximum inward extent, surface convection reaches $M_r = 0.3387\ M_\odot$ when the core mass is $M_1 = 0.2645\ M_\odot$ (mixing length = 1.5 times the pressure scale height). This deepest reach is much deeper than in a pure Population III model where, at its maximum inward extent, surface convection reaches only to $M_r = 0.5903\ M_\odot$ when the core mass is $M_1 = 0.3454\ M_\odot$. As a result of the first dredge-up event, the surface nitrogen abundance increases to $X_{\rm N} = 1.6 \times 10^{-6}$ at the expense of carbon, leading to the ratio ${\rm C/N} \simeq 100$, which is in the range consistent with the observations for HE 0107−5240. But ^{22}Ne hardly burns in layers that can be reached by the base of the convective envelope during the first dredge-up episode, and, hence, Na cannot be produced during evolution along the RGB phase of an isolated single star. One also cannot invoke extra mixing of the sort implied by abundances observed for some giants in globular clusters that are known to exhibit surface enhancements of sodium; such mixing brings about the depletion of carbon and the enhancement of nitrogen at the same time that it brings about enhancement of sodium. This may constitute an additional argument against the single-star scenario of Umeda & Nomoto (2003) (see § 2), which assumes birth out of a small cloud polluted with the ejectum of a supernova with an unusual carbon enrichment.

5. CONCLUSIONS AND DISCUSSION

During the past decade, there has been considerable observational and theoretical progress in understanding the properties of extremely metal-poor (EMP) stars in the Galactic halo. Thanks to the HK survey (Beers et al. 1992), the number of known EMP stars ($[{\rm Fe/H}] \lesssim -2.5$) has reached more than 100, and the spectroscopic characteristics of these stars have been revealed through detailed studies using large telescopes. By analyzing existing theoretical and observational evidence and by utilizing the results of new computations, we have focused in this paper on the peculiarities that distinguish EMP stars from Population I and Population II stars and have presented a general theoretical framework for understanding the evolution of EMP stars and for understanding the nucleosynthesis that has taken place in their interiors. Our framework relies heavily on a binary scenario in which the primary has produced, and transferred to the secondary, many of the isotopes that are present at the surface of an observed EMP star.

A distinct feature that characterizes the evolution of EMP stars of low- and intermediate-mass is the helium-flash–driven deep mixing (He-FDDM) phenomenon, which is triggered when the outer edge of a convective zone driven by a first helium-shell flash (which occurs near the beginning of the AGB phase in intermediate-mass models and at the tip of the RGB in low-mass models) extends into hydrogen-rich material. The first discussions of the He-FDDM mechanism (Fujimoto et al. 1990, 1995, 2000; Hollowell et al. 1990) drew attention to the surface enhancement of carbon and nitrogen made possible by this mechanism. In the present paper, we have investigated another consequence of the He-FDDM event, namely, the nucleosynthesis of *s*-process elements which occurs when neutrons are released by the reaction $^{13}{\rm C}(\alpha, n)^{16}{\rm O}$ in the helium- and carbon-rich convective zone.

We demonstrate that products of this nucleosynthesis can lead to surface enrichments of O, Ne, Na, and Mg and, if iron-group seed nuclei are present in the convective zone, to surface enrichments of heavy *s*-process elements. In addition, stars that evolve to the TPAGB phase after having experienced a He-FDDM event can also develop a large $^{12}C/^{13}C$ ratio at the surface in consequence of third dredge-up events.

Our binary scenario gives a reasonable account of the observed properties of EMP stars, such as the very high frequency of carbon-rich stars and *s*-process nucleosynthesis products that differ from those made by stars of younger populations. The scenario enables us in principle to identify modifications in surface abundances which, after birth in an unpolluted primordial cloud, first-generation EMP stars may have experienced due to accretion of primordial matter polluted by the ejecta of first-generation supernovae; this ability is essential if we wish to use low-mass EMP star survivors as tools to probe the early universe.

We have constructed a specific binary scenario to account for the observed abundance characteristics of HE 0107−5240. The initial binary system has the properties: separation ∼18 AU, orbital period ∼45 yr, a secondary of mass ∼0.8 $M_\odot$, and a primary of mass in the range $1.2 \lesssim M/M_\odot \lesssim 3$. The primary follows an evolutionary path of the case II′ variety in the classification scheme defined by Fujimoto et al. (2000). In consequence of experiencing a He-FDDM episode, the primary develops surface enhancements of C and N and, in consequence of experiencing third dredge-up events during the subsequent TPAGB phase, develops a large overabundance of C relative to N as well as enhancements of O, Ne, and Na, formed during the He-FDDM and subsequent thermal pulses. After ejecting its hydrogen-rich envelope in a superwind, the primary evolves into a white dwarf. The secondary accretes heavy-element enriched matter from the wind emitted by the primary and, when it evolves into a red giant, it mixes this enriched matter into a deep convective envelope, establishing surface abundance peculiarities similar to those observed for HE 0107−5240.

Because the iron abundance is so small ($[Fe/H] = -5.3$), the presence of iron-group elements in HE 0107−5240 can be attributed to either (1) accretion after birth of gas in a parent primordial cloud that has been polluted with material ejected by one or more first-generation supernovae or (2) birth out of already polluted matter in the parent cloud.

We have shown that further light on the source of iron-group elements can be shed by comparing an observed distribution of heavy *s*-process elements with theoretical expectations. An abundance ratio $[Pb/Fe] \simeq 1 \sim 2$, coupled with a large Pb/Ba ratio would be evidence that HE 0107−5240 is a second-generation star, or a Population III star in a binary with a primary of initial mass in the range $2.5 \lesssim M/M_\odot \lesssim 3.0$. A lack of heavy *s*-process element enrichment would indicate that HE 0107−5240 is really a Population III star in a binary with a primary component of initial mass in the range $1.2\ M_\odot \lesssim M \lesssim 2.5\ M_\odot$. Unfortunately, current observations provide only upper limits on the abundances of light and main-line *s*-process elements, so no conclusion can as yet be drawn. A ratio $[Pb/Fe] \simeq 1$–2 translates into a ratio $[Pb/H] \simeq -4 \sim -3$ for HE 0107−5240. This is difficult to detect with present facilities, and we will probably have to wait for future observations with a next-generation large telescope and the elaboration of model atmosphere including, for example, three-dimensional hydrodynamic simulations to establish definitively whether or not HE 0107−5240 is a Population III star.

With regard to the current binary status of HE 0107−5240, variations in the radial velocity of the size predicted by our scenario cannot be excluded by extant spectroscopic observations that, to date, cover only 52 days (Christlieb et al. 2004) and 373 days (Bessell et al. 2004). Because of wind mass loss, the initial binary system may have been considerably widened. Adopting Jean's theorem, which predicts the constancy of the product, semimajor axis times the total mass, we would expect the current binary to have the characteristics $a \simeq 34$ AU and $P_{\rm orb} \simeq 150$ yr, giving an orbital velocity of ∼7 km s^{-1}. Confirmation of such a small velocity demands long term observations at high dispersion.

As far as alternative single-star interpretations of HE 0107−5240 are concerned, any viable scenario must begin with formation out of gas with a singularly unusual abundance distribution (including the currently observed carbon and oxygen enhancements) of the sort not expected by mixing products of normal supernovae with primordial matter. As an example, a scenario proposed by Umeda & Nomoto (2003) supposes that the gas out of which HE 0107−5240 was formed acquired a carbon abundance of $[C/H] = -1.3$ after the mixing of an unusually small amount of primordial matter with a supernova ejectum in which the mass of carbon is $\simeq 0.2\ M_\odot$. Given that a typical type II supernova ejects a mass of the order of 0.1–1 $M_\odot$ in the form of Fe, a most peculiar process of star formation is required to account at the same time for a ratio of $[Fe/H] \simeq -3$ characteristic of EMP stars. It is to be noted that the mass of carbon in the supernova ejectum cannot be much larger than the mass of iron in the ejectum since, in order to obtain the observed C/O ratio, the carbon can only have come from the shell of partial helium burning existing above the region where iron-group elements are formed. In addition, since, in contrast with nitrogen, which can be produced in the interior and brought to the surface during the first dredge-up phase on the RGB, sodium cannot be formed during the evolution of a low-mass star, and a noncanonical mechanism for sodium enrichment has to be invoked. Given this hurdle for the (any) single-star scenario, it seems reasonable to accept the observed Na enhancement as evidence that some of the matter in the convective envelope of HE 0107−5240 was formed in the interior of a primary companion during the AGB phase.

Although there is a controversy as to whether or not a single-star of mass as small as that of HE 0107−5240 can be formed in a primordial cloud, a condensation as massive as the 2–3.8 $M_\odot$ predicted by our binary scenario is not excluded by current theory (Nakamura & Umemura 2001), which suggests a bimodal star-formation mass function for first-generation stars. The initial condensation could be formed as a first-generation object in the first collapsed, primordial cloud of total (dark and baryonic) mass $\sim 10^6\ M_\odot$. Another possible site is a primordial cloud of mass $\gtrsim 10^8\ M_\odot$, for which virial temperatures are higher than 10^4 K. In such a cloud, HE 0107−5240 could have been born as a first-generation star, but the formation epoch would be delayed in comparison with the formation epoch of first-generation stars in a lower mass collapsed cloud.

If HE 0107−5240 is a second-generation star, it also must have been formed in a cloud of total mass $\gtrsim 10^8\ M_\odot$. In a primordial cloud of total mass $\sim 10^6\ M_\odot$ and baryonic mass $\sim 10^5\ M_\odot$, contamination of primordial gas with the 0.1–1 $M_\odot$ of iron ejected by a typical supernova would produce an iron abundance $[Fe/H] = -3 \sim -2$. This metallicity is appropriate for most EMP stars known to date, but it is hundreds of times larger than the metallicity of HE 0107−5240. In order to

achieve a metallicity appropriate for HE 0107−5240, the contaminating supernova must eject an abnormally small mass of iron. But, the supernova explosion would be so weak that the remnant would dissolve into the interstellar gas instead of compressing it to collapse conditions, and star formation would not be triggered (Machida et al. 2004).

As described in the introduction, the history of the search for extremely metal-poor stars has taught us that, as the limiting magnitude of a survey is increased, stars of lower metallicity are detected, suggesting that, for EMP stars, there may be a correlation between typical metallicity and apparent luminosity, and hence, a relationship between typical metallicity and spatial distribution. In the current framework of structure formation, galaxies have been formed by the merging of lower-mass building blocks. If the parent cloud of HE 0107−5240 is of mass $\gtrsim 10^8\ M_\odot$, it differs from parent clouds of mass $\simeq 10^6\ M_\odot$ out of which many second-generation stars with $[\mathrm{Fe/H}] \simeq -4$ to ~ -2.5 may have been formed. Accordingly, in addition to commenting on initial abundances in primordial matter and characteristics of nucleosynthesis in supernova explosions in the early universe, EMP stars may also reveal the masses and locations in our Galaxy of their parent clouds.

The discovery of HE 0107−5240 has also demonstrated the importance of probing for Population III stars by sorting according to carbon-star characteristics rather than according to the weakness and/or absence of the Ca II K line. As pointed out by FII00, it makes sense to search for carbon stars since low-mass stars of $[\mathrm{Fe/H}] \lesssim -4.5$ spend their final nuclear burning lives as luminous carbon stars on the horizontal and asymptotic giant branches. Assuming that it has the luminosity of a typical red giant, HE 0107−5240 is at a distance of $\sim$10 kpc. Because the luminosity of a typical intermediate-mass TPAGB star is larger by about a factor of 10 than that of a typical low-mass RGB star, TPAGB stars are detectable at much larger limiting magnitudes than are RGB stars. The down side is that the lifetime of a typical TPAGB star is over 10 times smaller than that of a typical RGB star. Nevertheless, with CCD cameras, larger telescopes, and patience, we may be able to find Population III carbon stars further out in the Galactic halo and perhaps even in intergalactic space.

Recently, Margon et al. (2002) have reported a number of faint high-latitude carbon stars from the data obtained by the Sloan Digital Sky Survey (SDSS). Among these stars there may be EMP carbon stars of the sort that we suggest looking for, even though Margon et al. (2002) argue that nearby dwarf carbon stars outnumber giants in their sample. Follow-up spectroscopic observations may decide the issue. Since their selection is based on comparisons with known types of carbon stars in the five color system of SDSS (Krisciunas et al. 1998), there is the possibility that Population III carbon stars may be missed. Because of different atmospheric properties related to higher surface temperatures and different chemistry, the color properties of EMP carbon stars may differ significantly from those of more familiar carbon stars of Population I, or even from those of EMP carbon stars with $[\mathrm{Fe/H}] \simeq -3$. In any case, it is important to continue the search for carbon stars of low metallicities using every stratagem that can be devised, including methods that make use of spectral lines for which carbon molecules are responsible. From extremely metal-poor carbon stars found at extreme distances, or even from the absence of such stars, we may learn important information about the early universe.

We thank the referee, Norbert Christlieb, for valuable comments about the abundance of lead and for bringing to our attention the importance of predicting the carbon isotopic ratio. We also thank W. Aoki, N. Iwamoto, K. Nomoto, Y. Yoshii, and T. C. Beers for valuable discussions. This paper is based on one of the author's (T. S.) dissertation submitted to Hokkaido University, in partial fulfillment of the requirement for the doctorate. This work is in part supported by a Grant-in-Aid for Science Research from the Japanese Society for the Promotion of Science (grant 15204010). One of us (I. I.) thanks the Japanese Society for the Promotion of Science for an eminent scientist award, permitting an extended visit to Hokkaido University.

REFERENCES

Aikawa, M., Fujimoto, M. Y., & Kato, K. 2001, ApJ, 560, 937
Anders, E., & Grevesse, N. 1989, Geochim. Cosmochim. Acta, 53, 197
Aoki, W., Norris, J. E., Ryan, S. G., Beers, T. C., & Ando, H. 2000, ApJ, 536, L97
———. 2002a, ApJ, 567, 1166
Aoki, W., Ryan, S. G., Norris, J. E., Beers, T. C., & Ando, H. 2002b, ApJ, 580, 1149
Aoki, W., et al. 2001, ApJ, 561, 346
Alexander, D. R., & Ferguson, J. W. 1994, ApJ, 437, 879
Angulo, C., et al. 1999, Nucl. Phys. A, 656, 3
Bao, Z. Y., Beer, H., Kappeler, F., Voss, F., & Wisshak, K. 2000, At. Data Nucl. Data Tables, 76, 70
Beers, T. C., Preston, G. W., & Shectman, A. 1985, AJ, 90, 2089
———. 1992, AJ, 103, 1087
Bessell, M. S., Christlieb, N., & Gustafsson, B, 2004, ApJ, submitted (astro-ph/0401450)
Bessell, M. S., & Norris, J. E. 1984, ApJ, 285, 622
Bond, H. E. 1970, ApJS, 22, 117
———. 1980, ApJS, 44, 517
———. 1981, ApJ, 248, 606
Bondi, H. 1952, MNRAS, 112, 195
Bondi, H., & Hoyle, F. 1944, MRAS, 104, 273
Bromm, V., Coppi, P. S., & Larson, R. B. 1999, ApJ, 527, L5
Busso, M., Gallino, R., & Lambert, D. L. 1992, ApJ, 399, 218
Busso, M., Gallino, R., & Wasserburg, G. J. 1999, ARA&A, 37, 239
Carney, B. R., & Peterson, R. C. 1981, ApJ, 245, 238
Cassisi, S., & Castellani, V. 1993, ApJS, 88, 509
Cassisi, S., Castellani, V., & Tornambè, A. 1996, ApJ, 459, 298
Caughlan, G. R., & Fowler, A. W. 1988, At. Data Nucl. Data Tables, 40, 283
Chamberlain, J. W., & Aller, L. H. 1951, ApJ, 114, 52
Chieffi, A., Dominguez, I., Limongi, M., & Straniero, O. 2001, ApJ, 554, 1159
Chieffi, A., & Tornambé, A. 1984, ApJ, 287, 745
Christlieb, N., Gustafsson, B., Korn, A., Barklem, P. S., Beers, T. C., Bessell, M. S., Karisson, T., & Mizuno-Wiedner, M. 2004, ApJ, 603, 708
Christlieb, N., et al. 2002, Nature, 419, 904
Christlieb, N., Wisotzki, L., Reimers, D., Gehren, T., Reetz, J., & Beers, T. C. 1999, in ASP Conf. Ser. 165, The Galactic Halo, ed. B. K. Gibson, T. S. Axelrod, & E. Putman (San Francsico: ASP), 259
Cohen, J.G., Christlieb, N., Qian, Y.-Z., & Wasserburg, G. J. 2003, ApJ, 588, 1082
D'Antona, F. 1982, A&A, 115, L1
Depagne, E., et al. 2002, A&A, 390, 187
Fujimoto, M. Y., Iben, I., Jr., Chieffi, A., & Tornambé, A. 1984, ApJ, 287, 749
Fujimoto, M. Y., Iben, I. Jr., & Hollowell, D. 1990, ApJ, 349, 580
Fujimoto, M. Y., Ikeda, Y., & Iben, I., Jr. 2000, ApJ, 529, L25
Fujimoto, M. Y., & Sugimoto, D. 1979, PASJ, 31, 1
Fujimoto, M. Y., Sugiyama, K., Hollowell, D., & Iben, I., Jr. 1995, ApJ, 444, 175
Galli, D., & Palla, F. 1998, A&A, 335, 403
Gallino, R., Busso, M., Picchio, G., Raiteri, C. M., & Renzini, A. 1988, ApJ, 334, L45
Gallino, R., et al. 1998, ApJ, 497, 388
Gass, H., Liebert, J., & Wehrse, R. 1988, A&A, 189, 194

Goriely, S., & Mowlavi, N, L. 2000, A&A, 362, 599
Goriely, S., & Siess, L. 2001, A&A, 378, L25
Guenther, D. B., & Demarque, P. 1983, A&A, 118, 262
Haiman, Z., Rees, M., Thoul, A. A., & Loeb, A. 1996b, ApJ, 467, 522
Haiman, Z., Thoul, A.A., & Loeb, A. 1996a, ApJ, 464, 523
Heggie, D. C. 1975, MNRAS, 173, 729
Hill, V., et al. 2002, A&A, 387, 560
———. 2000, A&A, 353, 557
Hollowell, D., & Iben, I., Jr. 1989, ApJ, 340, 966
Hollowell, D., Iben, I., Jr., & Fujimoto, M. Y. 1990, ApJ, 351, 245
Hubbard, W. B., & Lampe, M. 1969, ApJS, 18, 297
Honda, S., et al. 2004, ApJ, 607, 474
Hoyle, F., & Lyttleton, R. A. 1939, Proc. Cambridge Phil. Soc., 35, 405
Iben, I., Jr. 1975, ApJ, 196, 525
———. 1977, ApJ, 217, 788
———. 1983, ApJ, 275, L65
———. 2000, in ASP Conf. Ser. 199, Asymmetrical Planetary Nebulae II: From Origins to Microstructures, ed. J. H. Kastner, N. Soker, & S. Rappaport (San Fransisco: ASP), 107
Iben, I., Jr., Fujimoto, M., Y., & MacDonald, J. 1992, ApJ, 388, 521
Iben, I., Jr. & Renzini, A. 1982a, ApJ, 259, L79
———. 1982b, ApJ, 263, L23
Iglesias, C. A., & Rogers, F. J. 1996, ApJ, 464, 943
Itoh, N., Hayashi, H., Nishikawa, A., & Kohyama, Y. 1996, ApJS, 102, 411
Itoh, N., Mitake, S., Iyetomi, H., & Ichimaru, S. 1983, ApJ, 273, 774
Iwamoto, N., Kajino, T., Mathews, G. J., Fujimoto, M. Y., & Aoki, W. 2004, ApJ, 602, 377
Johnson, J. A., & Bolte, M. 2002, ApJ, 579, L87
Krisciunas, K., Margon, B., & Szkody, P. 1998, PASP, 110, 1342
Limongi, M., Chieffi, A., & Bonifacio, P. 2003, ApJ, 594, L123
Lucatello, S., et al. 2003, AJ, 125, 875
Machida, M. N., Nakamura, F., Tomisaka, K., & Fujimoto, M.Y. 2004, ApJ, submitted
Margon, B., et al. 2002, AJ, 124, 1651
Marigo, P., Girardi, L., Chiosi, C., & Wood, P. R. 2001, A&A, 371, 152
Mathews, G. J., Bazan, G., & Cowan, J. I. 1992, ApJ, 391, 719
McClure, R. D. 1984, ApJ, 280, L31
McClure, R. D., Fletcher, J. M., & Nemec, J. 1980, ApJ, 238, L35
McWilliam, A. 1998, AJ, 115, 1640
Nakamura, F., & Umemura, M. 2001, ApJ, 548, 19
Nakamura, F., & Umemura, M. 2002, ApJ, 569, 549
Nishi, R., & Susa, H. 1999, ApJ, 523, L103
Norris, J. E., Ryan, S. G., & Beers, T. C. 1997a, ApJ, 488, 350
———. 1997b, ApJ, 489, L169
———. 2001, ApJ, 561, 1034
Omukai, K. 2000, ApJ, 534, 809
Omukai, K., & Nishi, R. 1998, ApJ, 508, 141
Omukai, K., & Yoshii, Y. 2003, ApJ, 599, 738
Palla, F., Salpeter, E. E., & Stahler, S. W. 1983, ApJ, 271, 632
Rees, M., J. 1976, MNRAS, 176, 483
Rossi, S., Beers, T. C., & Sneden, C. 1998, in ASP Conf. Ser. 165, The Galactic Halo, ed. B. K. Gibson, T. S. Axelrod, & E. Putman (San Francisco: ASP), 264
Ryan, S. G., Aoki, W., Norris, J. E., & Beers, T. C., Gallino, R., Busso, M., & Ando, H. 2001, Nucl. Phys. A, 688, 209
Ryan, S. G., Aoki, W., Norris, J. E., & Beers, T. C., 2003, ApJ, submitted
Ryan, S. G., Norris, J. E., & Bessl, S. 1996, ApJ, 471, 254
———. 1991, AJ, 102, 303
Sabano, Y., & Yoshii, Y. 1977, PASJ, 29, 207
Sackmann, I.-J. 1980, ApJ, 241, 37
Schlattl, H., Cassisi, S., Salaris, M., & Weiss, A. 2001, ApJ, 559, 1082
Schlattl, H., Salaris, M., Cassisi, S., & Weiss, A. 2002, A&A, 395, 77
Schneider, R., Ferrara, A., Salvaterra, R., Omukai, K., & Bromm, V. 2003, Nature, 422, 689
Shapiro, P. R., & Kang, H. 1987, ApJ, 318, 32
Shigeyama, T., Tsujimoto, T., & Yoshii, Y. 2003, ApJ, 586, L57
Siess, L., Livio, M., & Lattanzio, J. 2002, ApJ, 570, 329
Sneden, C., et al. 2003, ApJ, 591, 936
Straniero, O., et al. 1995, ApJ, 440, L85
Suda, T. 2003, Ph.D. thesis, Hokkaido Univ.
Tegmark, M., Silk, J., Rees, M. J., Branchard, A., Abel, T., & Palla, F. 1997, ApJ, 474, 1
Uehara, H., & Inutsuka, S. 2000, ApJ, 531, L91
Uehara, H., Susa, H., Nishi, R., Yamada, M., & Nakamura, T. 1996, ApJ, 473, L95
Umeda, H., & Nomoto, K. 2003, Nature, 412, 793
Van Eck, S., Goriely, S., Jorissen, A., & Plez, B. 2001, Nature, 412, 793
———. 2003, A&A, 404, 291
Wagner, R. L., 1974, ApJ, 191, 173
Weiss, A., Cassisi, S., Schlattl, H., & Salaris, M. 2000, ApJ, 533, 413
Yoneyama, T. 1972, PASJ, 24, 87
Yoshii, Y., & Sabano, Y. 1980, PASJ, 32, 229